DOE/BC/14893-10
(DE96001223)

INTEGRATION OF ADVANCED GEOSCIENCE AND ENGINEERING TECHNIQUES TO QUANTIFY INTERWELL HETEROGENEITY IN RESERVOIR MODELS

Annual Report for the Period
September 29, 1994 to September 30, 1995

By
F. David Martin
Jill S. Buckley
William W. Weiss
Ahmed Ouenes

April 1996

Performed Under Contract No. DE-AC22-93BC14893

New Mexico Institute of Mining and Technology
Socorro, New Mexico

Bartlesville Project Office
U. S. DEPARTMENT OF ENERGY
Bartlesville, Oklahoma

DOE/BC/14893-10
Distribution Category UC-122

Integration of Advanced Geoscience and Engineering Techniques to Quantify Interwell Heterogeneity in Reservoir Models

Annual Report for the Period
September 29, 1994 to September 30, 1995

By
F. David Martin
Jill S. Buckley
William W. Weiss
Ahmed Ouenes

April 1996

Work Performed Under Contract No. DE-AC22-93BC14893

Prepared for
U.S. Department of Energy
Assistant Secretary for Fossil Energy

Robert Lemmon, Project Manager
Bartlesville Project Office
P.O. Box 1398
Bartlesville, OK 74005

Prepared by
New Mexico Institute of Mining and Technology
New Mexico Petroleum Recovery Research Center
Socorro, NM 87801

TABLE OF CONTENTS

LIST OF FIGURES

LIST OF TABLES

ABSTRACT

The goal of this project is to provide a more quantitative definition of reservoir heterogeneity. This objective will be accomplished through the integration of geologic, geophysical, and engineering databases into a multidisciplinary understanding of reservoir architecture and associated fluid-rock and fluid-fluid interactions. The intent is to obtain a quantitative reservoir description incorporating outcrop, field, well-to-well, and laboratory core and fluid data of widely varying scales. This interdisciplinary effort will integrate geological and geophysical data with engineering and petrophysical results through reservoir simulation to quantify reservoir architecture and the dynamics of fluid-rock and fluid-fluid interactions. A more accurate reservoir description will allow greater accuracy and confidence during simulation and modeling as steps toward gaining greater recovery efficiency from existing reservoirs.

A field laboratory, the Sulimar Queen Unit, is available for the field research activities that are being conducted. Subcontractors from Stanford University and the University of Texas at Austin (UT) are collaborating in the research and are participating in the design and interpretation of field tests. Dr. Jerry Harris, Associate Professor in the Department of Geophysics at Stanford, is supervising the research and analysis of a crosswell seismic field experiment. Dr. Gary Pope, Director of the Center for Petroleum and Geosystems Engineering at the UT, is supervising the design and interpretation of a single-well wettability tracer test developed in his laboratories but not yet field tested. Several members of the PRRC staff are participating in the development of improved reservoir description by integration of the field and laboratory data as well as in the development of quantitative reservoir models to aid performance predictions.

The three-year project was initiated in September 1993. In the first year, subcontractor agreements with the University of Texas and Stanford University were submitted, modified, and executed. Pecos Petroleum Engineering Inc. in Roswell, NM, was retained as the field site agent.

Our initial approach in this work was to investigate crude oil/brine/rock (COBR) interactions under a variety of conditions, while comparing our results with other COBR systems, to make some estimate of reservoir wetting. In the first year of this work, we studied oil/brine and solid/brine interfacial properties, and oil/brine/solid interactions observed on flat surfaces. The second year was spent concentrating on oil/brine/solid interactions in porous media. Wax crystals were observed under reservoir conditions. Asphaltene also exists in small amounts. The connate brine is a nearly saturated salt solution, and pore surfaces were found coated with calcite or dolomite, all of which are important in understanding the crude oil/brine/rock interactions. A centrifuge study was conducted to establish a baseline, of two preserved core samples, to compare with other COBR interactions. Both core samples imbibe oil, and one sample also imbibed a significant amount of water. While not conclusive, these results indicate the existence of interconnected pathways of both water-wet and oil-wet surfaces, that is, mixed wetting reservoir conditions.

As mentioned in previous quarterly reports and the first annual report, the Single Well Wettability Tracer Test (SWWTT) design had changed significantly as a result of new information on wettability conditions and maximum injection and production rates. Results of a simulation of a four-layer model are outlined.

An outcrop study of the Queen Formation was conducted on the Rocky Arroyo and Bone Tank Draw exposures. It appears that Bone Tank Draw is more representative of Queen Formation. Porosity and permeability measurements were taken from collected rock samples. From these studies, it appears that the Shattuck Sandstone is not a single unit, where subunits are laterally continuous over the space of a single

outcrop. Geostatistical analysis will be used to determine the amount of spatial variation in the subunit petrophysical properties. Regarding the Subsurface Studies, all well data has been entered into the Landmark Graphics database and a series of structural contour and thickness maps have been generated for interpretation.

The geophysical data, resulting from the crosswell tomography experiment that was conducted in December 1994, was processed to obtain a velocity tomogram and a reflection image. A significant effort was devoted to tube wave attenuation, which consists of removing the tube wave noise embedded in the recorded signals. Using the new signals and the P-wave sonic log from Well 1-16, first arrival times were picked. Finally, a reflection image was derived after a wavefield separation using a Common Mid-Depth Gather (CMG).

In reservoir modeling, a procedure has been established to estimate porosities. Old style neutron logs and gamma ray logs have been correlated to core porosities that were available at five wells. Three of the wells were located in the Double L field located few miles North of the Sulimar Queen. Using a neural network and the available core porosities, the correlation between old logs and core porosities was used to estimate the porosity in most of the Sulimar Queen wells. These porosities will be used in constructing a reservoir model.

EXECUTIVE SUMMARY

The purpose of this project is to conduct a variety of laboratory and field tests and utilize all the geological, geophysical, and engineering information to develop a mathematical model of the reservoir by the use of global optimization methods. This interdisciplinary effort will integrate advanced geoscience and reservoir engineering concepts to quantify interwell reservoir heterogeneity and the dynamics of fluid-rock and fluid-fluid interactions. The reservoir characterization includes geological methods (outcrop and reservoir rock studies), geophysical methods (interwell acoustic techniques), and other reservoir/hydrologic methodologies including analyses of pressure transient data, core studies, and tracer tests. The field testing is being conducted at the Sulimar Queen Unit with related laboratory testing at the PRRC on samples from the Sulimar site and Queen sandstone outcrops. The aim is to 1) characterize and quantify lithologic heterogeneity, 2) mathematically quantify changes in heterogeneity at various scales, 3) integrate the wide variety of data into a model that is jointly constrained by the interdisciplinary interpretive effort, and 4) help optimize petroleum recovery efficiencies.

INTRODUCTION

Understanding how heterogeneity between wellbores affects flow through reservoirs and quantifying the effects requires further developments in reservoir characterization. The integration of engineering and petrophysics with geology and geophysics through reservoir simulation is necessary to improve the ability to understand well-to-well type heterogeneity. In particular, there are opportunities to combine techniques such as pressure transient testing and tracers that can be directed at improved understanding of interwell reservoir heterogeneity. Some of these techniques are well known, but they are being expanded to provide

new information: for example, a novel technique to look at wettability by the use of tracers. Other technologies are emerging in this area, especially pertaining to some of the geophysical means, such as crosswell tomography, as well as interdisciplinary approaches in reservoir management, and measures to quantify reservoir heterogeneity.

In order to maximize oil production from known reservoirs, an understanding of reservoir structures and the development of measures to characterize heterogeneities are essential. The physical phenomena involved with oil recovery have been relatively well understood for some time. Nevertheless, there have been disappointing gaps between laboratory, field, and computer research and the production of residual oil because of a lack of evaluating these techniques in controlled reservoirs and developing an understanding of the manner in which heterogeneities cause oil to be trapped. The scarcity of detailed reservoir data contributes to this break in continuity. A research field laboratory, available to the proposers of this project, and the synergism resulting from interdisciplinary research activities at a common site, presents a unique opportunity to conduct and validate the research needed for improved reservoir characterization.

DISCUSSION

This report describes work performed during the second year of the project. Separate discussions are provided for each of the task areas. The integration of results from the separate tasks into the final reservoir characterization will be accomplished during the coming year.

SULIMAR QUEEN RESERVOIR WETTABILITY

The Sulimar Queen project presents an opportunity to study reservoir wetting of a relatively light, waxy oil. Several factors make this an interesting case from the standpoint of understanding the crude oil/brine/rock interactions that are expected to control wettability.

- The oil contains significant amounts of both asphaltenes (about 4%) and paraffins (2.8%).
- Reservoir temperature (32°C) is less than the cloud point of the produced oil (57°C).
- The connate brine is a nearly saturated salt solution.
- Calcite or dolomite coatings are commonly observed on pore surfaces.

A centrifuge study has been conducted with two preserved core samples to establish a baseline to which other wettability testing can be compared.

Preserved Core Studies—Centrifuge

Capillary pressures and relative permeabilities were measured by Westport Technology Center International (WTCI) using the centrifuge technique. Two samples were taken from sections of preserved Sulimar Queen Core. The sealed core packages were examined by CT scanning to find the least heterogeneous sections. Two of these (1996.1 - 1996.4 ft and 1998.0 - 1998.4 ft) were opened and core plugs drilled in the most homogeneous portions of the whole core, also based on the CT images. Physical properties of the core plugs (dimensions, porosity, permeabilities) are given in Table 1.

Core plugs were flushed with synthetic reservoir brine (Table 2) diluted to 3/4 strength. The dilution was chosen to preserve the ratios of ions present in the reservoir brine, but to avoid the possibility of precipitation from the nearly saturated, full strength brine. No further cleaning of the preserved core plugs was attempted.

Displacements were performed beginning with the flushed cores as outlined in Table 3. These included measurements of water/oil and gas/oil capillary pressure curves and relative permeabilities. Data and models used to fit centrifuge data, resulting in the capillary pressure and relative permeabilities reported are discussed in more detail in the report provided by WTCI (Report No. WTCI-95-125). P_c and k_r results are shown in Figs. 1 and 2.

The results of the centrifuge tests, with respect to the wettability of the preserved core samples are included in Table 1. I_w and I_o are the Amott indices to water and oil respectively and are defined as the ratio of water or oil that imbibes spontaneously to the total shift in saturation by spontaneous and forced displacement. In this case, the spontaneously imbibed volume is approximated by spinning the samples at very low speed. The combined Amott-Harvey index is given by:

$$I_{AH} = I_w - I_o$$

The final wettability measure in Table 1 is the USBM index, I_{USBM}, which is the ratio of the logs of the areas under the Pc curves from steps 1 and 2 in Table 3.

Both core samples imbibe oil, giving estimates for I_o of more than 0.5. One of the samples also imbibes a significant amount of water. The Amott-Harvey and USBM indices both indicate preferentially oil-wet behavior.

Mixed-wet is perhaps a more accurate description of wetting in these cores since one imbibes both water and oil. Mixed wetting implies that some surfaces are preferentially water-wet and others are more oil-wet. The fact that both fluids imbibe demonstrates the existence of interconnected pathways of both water-wet and oil-wet surfaces. It should be emphasized that this evidence is not conclusive vis-à-vis the reservoir since disturbances in temperature, pressure, and brine composition have all had an opportunity to change wetting during the period of storage of the preserved core. Nevertheless, it is the best available estimate of reservoir wettability and fits well with currently accepted views on reservoir wetting.[1]

Preserved Core Studies—Spontaneous Imbibition

The Amott indices reported above were calculated by assuming that the volume of fluid that imbibes spontaneously is closely approximated by the volume of that fluid expelled at a low rotational speed. This method has the advantage of being much faster than spontaneous imbibition into weakly-wetted cores, but no rigorous comparisons are available to show how good an approximation this is. The rate of spontaneous imbibition can also be used as an indication of wetting.[2] These tests are, of course, much slower, especially in low permeability cores. In Table 4 are listed the physical properties of four core plugs, two from preserved core sections and two from unpreserved sections of the whole core. Each core plug was flushed with 3/4 strength reservoir brine. Figure 3 shows the rate of imbibition of oil (a mixture of 1/5 toluene and 4/5 paraffin oil with density of 0.863 g/ml and 12 cp viscosity) into these four core plugs. The two preserved cores imbibe oil readily whereas no oil is taken up by either of the unpreserved cores.

Surface Studies with Produced Oil

It is now widely accepted that oil reservoirs can have a range of wetting conditions that depends not only on the oil and rock, but also on the composition and amount of the brine phase. Factors that can influence the extent of wetting alteration in COBR ensembles include the chemical compositions of the crude oil, brine, and mineral surfaces, as well as the duration of contact between these phases and the temperature during the aging period. In cores, the brine saturation is important as well .[3] Circumstances under which adsorption occurs, the extent to which wetting is changed, and the possibility that adsorption of crude oil components is reversible, have been reported for smooth surfaces and an asphaltic crude oil.[4]

Mixed wetting is envisioned as arising from two sources: chemical heterogeneity of pore surface and initial distributions of oil and water in the pore space. Chemical heterogeneity of pore surface material certainly can cause different COBR interactions on different surfaces. Patchy mixed wetting can be generated by this mechanism, but it is harder to explain interconnection of the pathways of oil-wet and water-wet surfaces if they occur primarily because of surface chemical heterogeneity. A second mechanism that leads to the generation of mixed-wet conditions depends on the initial distribution of oil and water in the pore space and subsequent interactions between crude oil components and exposed rock surfaces as illustrated schematically in Fig. 4 for a pore of triangular cross section.

The triangular pore shape incorporates an important aspect of pores that is overlooked in the early capillary tube models where cylindrical cross sections were generally assumed. Pores with corners retain wetting phase as shown in Fig. 4b. There would also be thinner films of water all along the pore surfaces. Whether these water films are stable, and thus whether adsorption can occur and mixed-wetting develop, depends on the compositions of all three phases: solid, brine, and oil. For the Sulimar Queen reservoir, surface studies have concentrated on silicate surfaces, produced crude oil, and both NaCl and synthetic reservoir brines, as summarized in Table 5.

Contact angles measured with distilled water and decane were generally lower than those reported for other crude oils for similar conditions of brine composition, aging temperature, and aging times.[4] The highest water-advancing angles for slides pretreated with brine before aging in crude oil were all less than 90 degrees. In general, the highest (pH 8) and lowest (pH 4) brine treatment led to higher values of θ_a, than did brines with pH near 6.

Even on dry glass, contact angles were lower than for other oils. As shown in Table 6, raising the aging temperature of the oil to 80°C above the cloud point of the produced oil and maintaining that temperature for five days did not increase θ_a. If, however, the oil and glass were allowed to cool back to room temperature and the aging time continued, θ_a began to increase. The highest value of θ_a observed was 145 degrees after 22 days of additional aging at room temperature.

HYDROLOGIC AND TRACER RESEARCH (UNIVERSITY OF TEXAS)

The design for the SWWTT for the Sulimar Queen Field has changed significantly from what we reported in our last annual and progress reports. The design was changed due to new information such as the wettability conditions and maximum injection and production rates available to us from the field and laboratory tests. Here we report on the results of a simulation of a four-layer model using ethyl formate and propyl formate as the reacting tracers in a weakly water-wet media. The injection rate of 15.5 bbls/day and

the production rate of 8 bbls/day are used. The production rate is significantly lower than what we used in our earlier design calculations.

Reservoir Properties

The permeability, porosity, and initial saturation used in the simulation are estimated based on the core data and are given in Table 7.

Estimated initial oil-in-place for the Sulimar Queen Field in Chaves County, New Mexico is 6.33 MMSTB with 2.77 MMSTB as the movable oil and 3.56 MMSTB as the residual oil. Current average oil saturation for the reservoir is estimated at 39% and the movable oil saturation is about 5%. Static reservoir pressure at 1995 ft is 719 psia and the pressure gradient is 0.495 psi/ft. The cap rock is 4 to 6 ft of anhydrite and the reservoir rock is sandstone and silt stone (Shattuck sand) about 11 ft thick. There is a 1 ft shale at the depth of 2005 ft with a permeability of about 0.3 md. We excluded this shale layer in our simulations and thus the effective reservoir thickness of 10 ft was used.

The SWWTT is designed for Well number 1-16 in the Sulimar Queen Field. This well was drilled in August 1990 with the total depth of 2065 ft. The well is perforated for 11 ft from the depth of 1995 ft to 2006 ft. The casing diameter is 5 1/2 inches with 2 3/8 inch tubing. The ground level of the well is 3958 ft above the sea level.

Fluid Properties

The API gravity of Sulimar Queen crude oil is 35° and thus the density is 0.85 g/cc at 60° F and 0.834 g/cc at the reservoir temperature of 86° F. The oil viscosity is 7.67 cp at the reservoir temperature. The density of formation water is 1.141 g/cc and its viscosity is 1.51 cp at the reservoir temperature. Total dissolved solids in the formation water is about 308 g/L. The brine-oil interfacial tension is 21 dynes/cm.

SWWTT Design for Sulimar Queen Field

One of the most important SWWTT design factors as indicated in our earlier reports is how long the test should last, which is a function of the injection and production rates. The length of the test affects how much time the reactant tracers have to hydrolyze into the product tracers. Therefore, too long a time would make the reactant tracer peak concentration too small to measure. There are two factors that affect the time, namely slug size and the shut-in time, if needed. The slug size should be as large as possible to increase the sweep in the reservoir and push the slug farther away from the wellbore, yet small enough to reduce the length of the test, thus producing product tracer at measurable concentrations. We can accurately measure the alcohol concentrations down to 10 ppm using gas chromatography.

The water tracers used in this design are reacting ethyl formate with the product tracer of ethanol and methanol as a nonreacting tracer. The tracers used with the oil slug are reacting propyl formate tracer with the product tracer of normal propyl alcohol. The nonpartitioning nonreacting oil tracer used is octanol. The tracer properties such as partition coefficients and reaction constants are given in Table 8. The sequence of fluids injected and the time period for each slug are given in Table 9. The injection concentration and amount of tracers are given in Table 10.

Figure 5 shows the timeline for this base case SWWTT design. Injected water is 60 bbls and injected oil is 80 bbls. There is no shut-in time used in this design due to low maximum production rate of 8 bbls/day and in consequence the long residence time for the reacting tracers.

The reservoir and fluid data used in the simulation are given in Table 11. The wettability was assumed to be weakly water-wet in this base case SWWTT simulation. The residual saturations are 0.34 for both water and crude oil. The relative permeability and capillary pressure curves are calculated assuming Corey-type functions (Figs. 6 and 7). The capillary pressure shown in Fig. 7 is computed based on average properties of permeability of 50 md and porosity of 0.19. However, the capillary pressure is calculated for the gridblock permeability and porosity during the simulation. The endpoint relative permeabilities are 0.35 and 1 with the exponent of relative permeability curves of 1.4 and 2.3 for water and oil, respectively. The capillary pressure endpoint and exponent are 15 psi $(darcy)^{0.5}$ and 4.

The water-cut and the bottomhole pressure are shown in Figs. 8 and 9. The tracer response curves are shown in Figs.10–13 with the following peak concentrations:

Tracer	Peak Concentration (ppm)
MeOH	3,327
EtFr	1,679
EtOH	7,277
OcOH	5,001
PrFr	2,595
NPA	1,646

With this design, the tails are easily detected and the tracer concentrations are well above the detection limit of 10 ppm. The length of the SWWTT will be at least 55 days. It is possible to shorten the test but that will make it less likely that we get a good measure of the tracer tails.

GEOLOGICAL STUDIES

Field Studies

An outcrop study of the Queen Formation was conducted on exposures in two major areas; Rocky Arroyo, and Bone Tank Draw. Field locations are about 40 miles southwest of the Sulimar Queen Field and approximately 10 miles west of the location of the Goat Seep Reef margin during time of deposition (Fig. 14). The objectives of the study were to collect quantitative information on dimensions and geometries of sand bodies, and to determine what kinds of barriers to fluid flow might be present, the spatial distribution of porosity and permeability, and what factors control their distribution.

During the past year, numerous rock samples were collected for permeability studies. Because of difficulties encountered when using the field minipermeameter, we elected to collect rock samples and return them to the lab for permeability and porosity measurements. Most samples were obtained using a portable

rock drill provided by the New Mexico Bureau of Mines and Mineral Resources. Use of the drill allows collection of samples that are more free of surficial weathering effects, and allows for sampling of highly indurated rocks. Additionally, by collecting samples to take to the lab rather than making field permeability measurements, the miniporo-permeameter at the PRRC can be used to make very detailed measurements of permeability and porosity variation. The same samples can also be examined using petrographic techniques to determine relationships between petrophysical and rock properties.

Rocky Arroyo

In the study area, Rocky Arroyo runs east-west, therefore most of the outcrops studied run perpendicular to the Goat Seep shelf margin (Fig. 14). One small section was perpendicular to the main trend of Rocky Arroyo, so this section runs parallel to the reef margin. Five sections of the Queen Formation were measured and described. Figure 15 shows the locations of the various measured sections.

The longest section, and the one studied in most detail was Section 2, shown in Figs. 16a and 16b. This section runs east-west along the south wall of Rocky Arroyo, and has a lateral extent of about 500 ft. Thirty to thirty-five ft of the Shattuck sandstone is exposed here, and the exposure can be divided into 6 different units, based on lithology and permeability. Sandstones are light gray to yellowish tan and fine to very fine-grained. Sedimentary structures are rare, but include parallel and wavy laminations and minor crossbedding. The upper part of some bedding surfaces contains desiccation cracks and gypsum rosettes, indicating deposition very near the sediment-water interface and periodic exposure to subaerial conditions.[5] The best-exposed portions of Section 2 were sampled on an interval of 10 ft horizontally and two ft vertically; it is believed that this interval should reveal most heterogeneities within the sampled section. Permeabilities range from less than 1 md to 176 md for Section 2; some units show much greater permeability variation than others. Lowest permeabilities were seen in a lens-shaped massively-bedded unit that has been interpreted variously as dune foresets[6] or lagoonal sand waves,[7] while much higher permeabilities were seen in an upper unit that contained evidence of deposition in very shallow subaqueous to supratidal environments. The low permeability sandstones are clean, well-sorted, very fine grained sands that have been tightly cemented with carbonate and quartz cements. Two clay-rich layers were present in this outcrop, these also had low permeabilities and act as aquitards of groundwater flow. Preliminary grain size analysis of Section 2 shows that there is an overall positive correlation between grain size and permeability in this outcrop (Fig. 16b).

Bone Tank Draw

The Bone Tank Draw section (Section 7, Fig. 15) is exposed in Bone Tank Draw near Lee Ranch. This outcrop is about 7 mi to the northwest of Section 2. It was located about 16 mi landward of the position of the Goat Seep reef (Fig. 14) during time of deposition, further than any of the other outcrops studied. The Sulimar Queen field is about 20 mi north of the Goat Seep Reef, and exhibits relatively different facies and depositional environment from the outcrops studied in Rocky Arroyo; however, it is quite similar to the outcrop in the Bone Tank Draw section.

Figure 17 shows a schematic measured section description of the Bone Tank Draw section. The Shattuck outcrop in Bone Tank Draw is about 11 - 15 ft thick of sandstone, overlain and underlain by massive

and bedded gypsum interbedded with red siltstone. The sands can be divided into four thin units that persist throughout the outcrop area. Sedimentary structures include parallel or subparallel laminations, flaser bedding, and occasional wavy bedding similar to that seen in the Sulimar reservoir rocks. Permeabilities are generally low in much of the sandstone, averaging about 5 md, however there is one poorly cemented sandstone layer with an average permeability of 140 md. This layer is laterally continuous throughout the Bone Tank Draw outcrop but varies in thickness, thickening to the south.

One feature that has become apparent from the outcrop permeability studies of the Rocky Arroyo and Bone Tank Draw outcrops is that the Shattuck sandstone is not a single unit, but can be divided into smaller subunits based on variations in lithology, sedimentary structures, depositional environment, and, ultimately, permeability. Based on observation of groundwater flow at the outcrop face, there is definitely preferential fluid flow within some layers. It may be possible to relate the various units seen in outcrop to similar units seen in the subsurface, and this information will be incorporated into the reservoir models of the Sulimar Queen field.

Another conclusion that can be drawn from outcrop studies is that although individual units are laterally continuous over the space of a single outcrop (a few hundred ft at most), it is quite difficult to correlate units over distances of several hundreds of ft. Geostatistical methods should provide an estimate of the spatial variation in petrophysical properties.

Subsurface Studies

All well data has now been entered into the Landmark Graphics database. Figure 18 shows a base map of the Sulimar Queen field, with well spots and the position of a two-dimensional (2–D) regional seismic survey marked. Figure 19 is a structural contour map, made on the top of the Shattuck sand or upper pay zone of the Queen. The Queen sandstone in the Sulimar field is distinguished in well logs by a high gamma ray response due to the high feldspar content of Queen sandstones. The Queen top was picked at the inflection point in the gamma ray log where this strong positive response is noted. Structure on the top of the Shattuck shows a regional dip from the NW to the SE part of the field, with three structural nodes that stand out from the regional structural trend. The regional dip varies from 30 to 100 ft per mile. Structure maps on top of the overlying Seven Rivers and Yates Formations are very similar, indicating that current structural trends are probably post-Permian in nature.

Figure 20 shows a gross sand thickness map for the upper Queen pay zone. Sand thickness for this map was determined from electric logs or from previously published data where logs were not available. A bottom pick for the pay zone was difficult to make, as some of the gamma ray logs did not actually extend to the bottom of the hole; in these cases the pick was made from the neutron log, or previously published perforation data if no other means was available. Gamma ray tool resolution is not sufficient to distinguish small interbedded siltstones and shales within the coarser sand body, so no net pay sand map was generated. Current work is in progress that will attempt to use neutron log data for pay zone determination and refinement of internal reservoir structure. Figure 21 overlays the structural contour map onto the sand thickness map, showing that in general, the sands are thicker in the northeast part of the field, and that there seems to be no strong structural control over sand thickness. These maps differ somewhat from previously published maps,[8] particularly the sand thickness map. This may be because the thicknesses shown in Fig. 20

are derived primarily from log data, whereas those in the preliminary study are from scout reports, logs and cuttings. None of these methods can provide truly accurate thickness measurements, particularly on such thin units as the Shattuck sandstone. Also, log picks depths may vary depending on whether one uses an inflection point or a cutoff value as the pick point.

Figure 22 is another base map of the field, this one showing the locations of a number of structural cross-sections that were made for the field. Figures 23–24 are structural cross-sections drawn across the field. From these, one can see the general rise in elevation towards the western part of the field, as well as the thickening of the sand body in the central portion of the area. There are a few local highs and lows, also seen on the structure map, but relief is quite low across the field and generally follows the structural trend of the area.

GEOPHYSICAL RESEARCH (STANFORD UNIVERSITY)

Acquisition

The New Mexico Queen crosswell field experiment began on December 18 and was completed on December 21, 1994. A complete dataset of approximately 10,000 traces (100 x 100) was acquired with no major equipment or acquisition problems. We encountered significant tube wave noise and apparently low signal level due to high attenuation in the shallow and low pressure reservoir. To address the tube wave problem, the source and receiver wells were switched. After switching the source and receiver wells, there was some improvement in data quality.

The survey was recorded with 5 ft source and receiver vertical spacing instead of the 3 1/3 ft spacing desired. This reduction in sampling was necessitated by the poor signal to noise ratio and the fixed budget. Two receiver gathers at 1700 and 1750 ft were collected at 1 ft. spacing in order to test the effect of coarser sampling during the data processing. These two gathers might also give us a benchmark or reference that can be used for the entire data set. Figure 25 shows the geometry of the survey.

Field Data. The data recorded in the field were generated by a linear source sweep from 350 Hz - 2000 Hz. Before we can start analyzing the data, we must correlate it with the source sweep. We do this by cross correlating all of the traces with the linear source sweep from 350 Hz - 2000 Hz. Figure 26 shows a receiver gather of the raw data after cross correlation.

Processing Objectives

In crosswell seismic imaging, the objective is to use the sound signal emanated from the source well and recorded within the receiver well to interpret the medium between the two wells. Our primary objective with the Queen crosswell survey data set is to obtain two types of images or sets of information as a function of position within the medium: 1) a velocity tomogram, and 2) a reflection image.

A velocity tomogram yields localized information on the velocity at which sound propagates through the medium. Different types of rocks allow sound waves to propagate through them at different speeds. A reflection image yields localized information on the impedance contrasts within the medium. Therefore a reflection image can tell us where the geological structure of the medium is changing. Tomography uses the traveltime of the direct arrival, and reflection mapping uses the full waveform of the reflection arrivals. Tomography is the low wavenumber resolution of the medium, and reflection imaging is a higher wavenumber resolution of the medium. Figure 27 shows the geometry of the direct and reflected arrival raypaths.

Preliminary Processing

Full waveform crosswell data are very complicated. The field data contain many different wavemodes. We have to go through a series of processes to obtain useful information from the data. We start this process by correlating the data with the source sweep, and tube wave attenuation.

Tube Wave Attenuation. The data contain strong tube wave noise. The tube wave is the wavetrain that propagates within the borehole, and then hits a perforation at the top or bottom of the well casing and propagates toward the receiver well. Tube waves are one of the main sources of noise within a crosswell survey. Before we can do any processing for tomography or reflection imaging, we need to attempt to remove as much of the tube wave noise as possible. We can take advantage of the fact the moveout of the tube waves in source and receiver gathers is close to linear, and that the waveform and frequency content of the tube waves is nearly constant. Within source and receiver gathers, we have performed a trace mix subtraction operation along the moveout of the tube wave. This is a convolutional operator in space over a moving window of traces. The size of the trace mix window is the size of the convolutional operator and has a large effect on the data. Several different window sizes were tried, and the optimal window size was chosen. After this trace mix procedure we have reduced the tube wave noise. This makes it easier to do additional processing. Figure 28 shows a receiver gather after tube wave noise removal. We see the tube wave was removed and a significant difference in the data quality.

Tomography

Tomography is based on the traveltime of the direct arrival. The traveltime of the direct arrival is directly related to the velocity of the medium by:

$$v = l / t \tag{1}$$

where l is the length of the direct arrival raypath , v is the average velocity of the medium along the raypath, and t is the traveltime of the raypath. By simultaneous inversion of Eq. (1) for all the traveltimes of the direct arrivals from all source - receiver pairs, we can solve for the velocity at various points between the wells.

Picking the first arrival. Before we can perform traveltime tomography, we have to pick the direct arrival traveltimes from the recorded time series for each source - receiver pair. The ideal first arrival has a strong

peaked wavelet. We need to have a reasonably strong direct arrival to make an accurate traveltime pick of the direct P-wave. While we can't see a clear first arrival on most of the traces, we can see a general envelope of the wavefront; particularly in the common offset gathers (COG) where the difference in the receiver and source depths are held constant). This indicates velocity variation within the survey as a function of depth. However, we need a well-defined first arrival, and additional information to calibrate or justify the first arrival picks. Therefore we have used some additional tools to help us with the first break picking. We have done the following: (1) calculated the analytical signal of the data and (2) modeled where we expect the first arrival to be by using the sonic logs to do some synthetic modeling of the expected wavefield.

In order to further enhance the emerging wavefront, we have calculated the modulus of the analytical signal of the data (Fig. 29). The modulus of the analytical signal gives the envelope of the full waveform data. The analytical signal is a function of the original data and the Hilbert transform of the data. This gives an improved definition to the emerging wavefront.

In order to see if there is any correlation between the traveltime of the emerging wavefront and the expected traveltime of the direct arrival, we have done synthetic traveltime modeling based on the P-wave sonic log from Well 1-16. The sonic log was picked every 10 ft for velocities. This gave us a preliminary velocity model for synthetic traveltime modeling. We then smoothed this velocity model by a moving triangular window consisting of 3 points with weights (1, 2, 1). The resulting velocity (slowness) model is shown in Fig. 30. We then used a raytracing program to calculate traveltimes as a function of source-receiver position. For the modeling, we used a constant well spacing (i.e. no well deviations were included). The synthetic traveltimes are shown in Fig. 31. Figure 32 shows the synthetic traveltimes for the zero offset gather (the zero offset gather is the group of source-receiver pairs that have the same depth). We see traveltime variation within this gather, indicating a change in seismic velocity with depth.

Tomography Results. Using the sonic log modeled traveltimes as a guide, we picked the direct arrival traveltimes in COGs. We picked the gathers with offsets from -20 to +20 ft. The COGs outside this range were unpickable because of poor data quality. After picking the traveltimes, we inverted them to find the velocity structure of the medium. We used 280 ft for the well spacing. The resulting 1–D velocity inversion is shown in Fig. 33.

Reflection Processing

As stated previously, the reflection image is an image of impedance contrasts of the medium convolved with a wavelet representing the impulse response of the medium. Before we can do any reflection imaging, we have to separate the reflected energy from the undesired noise as completely as possible.

Wavefield Separation. Reflection imaging is based on being able to separate the desired reflection energy from rest of the complex crosswell wavefield. The difficulty of this depends on the signal-to-noise ratio of the data. This is a function of well spacing, source strength and bandwidth, reservoir pressure, and p and s wave velocities. As discussed earlier, we have already done some wavefield processing (cross correlation and tube-wave attenuation). For reflection imaging, we have to do additional wavefield processing. Each individual dataset has its own unique wavefield separation problems.

In multiple-fold crosswell reflection imaging, we can take advantage of the different ways that data

can be sorted. There are four basic domains in which we can sort crosswell data: Common Source Gather (CSG), Common Receiver Gather (CRG), Common Offset Gather (COG), and Common Mid-depth Gather (CMG).They are described as follows:

(1) CSG - gather of all traces for one source depth.

(2) CRG - gather of all traces for one receiver depth.

(3) COG - gather of all traces for which the difference of the source depth and receiver depth are held constant.

(4) CMG - gather of all traces for which the sum of the source depth and receiver depth are held constant.

Various wave modes have different moveouts depending on the domain in which the traces are sorted. We can use this to find the best domain for filtering the undesired types of noise. As stated previously, we did tube wave-attenuation in Common Source and Receiver Gathers. The filters we used are trace mixing, f-k and median filters, and temporal bandpassing. The COG has certain properties that make it useful for wavefield separation. In this gather, the direct arrival has linear moveout and the reflection arrivals have hyperbolic moveout. Therefore, we can remove noise due to the direct arrival by mixing and subtracting along zero moveout. We then f-k filter to try to enhance reflections. We try several different f-k filters of different widths to judge their effect on the data. The f-k filter is a powerful filter to remove noise. However, by passing the data too narrowly in f-k space, we can mix noise and signal, therefore creating artificial events in the data. Through a range of f-k filters widths, we look for events that are stable, and that have coherency with as wide an f-k pass as possible. Additionally, we have to choose an f-k filter that will separate upgoing and downgoing reflection arrivals. Figure 34 shows a common receiver gather after wavefield separation with upgoing reflections enhanced. It is possible that many of the events shown in Fig. 34 are S-wave reflections.

Reflection images. Figure 35 shows a reflection image after wavefield separation over a limited stack of CMGs from 1660 ft to 1720 ft. Figure 36 shows a reflection image over the optimal incidence angle range. Figure 36 shows a strong reflection that correlated well with the velocity image's large change in velocity at a depth of 1750 ft. The reflection images were created by Tomoseis Inc. The processing done by Tomoseis makes heavy use of the CMGs to do intermediate analysis on the wavefield separation quality, and the angle of incidence of the reflected raypath. The recorded wavelet of the reflection data has properties which change with the angle of incidence. The most important of these properties is the stretch of the wavelet attributed to the non-linear moveout correction. The reflection imaging procedure used the XSP-CDP mapping algorithm, which maps a sample on the recorded time series into a point in image space. A 1–D velocity model from tomographic inversion is used to do the mapping from time to image space.

RESERVOIR MODELING

The characterization of the Sulimar Queen field requires that the field porosity distribution be estimated with a fair level of confidence. Core porosity is considered to be one of the best indicators of this reservoir property. Unfortunately, for the Sulimar Queen, core porosities are available only in two wells. Furthermore, the only available logs are old style neutron and gamma ray logs. This lack of information on a field scale led us to predict the field porosity distribution using contemporary artificial neural network techniques.

The neural net is commonly referred to as an "equation generator." The human mind is capable of visualizing complex functional correlations in three-dimensional space. However, as the functional relationships between the given data (e.g., neutron readings) and the required outputs (e.g., porosities) becomes highly multi-dimensional, multivariate statistical modeling or artificial intelligence must be applied. In this specific study, we chose to use the Feedforward Backpropagation Neural Net (FFBP). This choice was made because the PRRC has already developed and tested the algorithm for this neural net.[9] In the following paragraphs, a brief introduction to the backpropagation network is presented.

Feedforward Backpropagation (FFBP) Neural Net. The human brain consists of a number of interconnected processing elements called neurons. During the temporal brain development, depending on the stimuli that influence this development, the neuronal pathways modify themselves so as to "learn" from this external stimuli. A neural network emulates this learning process in a rudimentary fashion.

The FFBP neural net, much like the brain, also consists of the interconnected processing elements (neurons). The formal training of the neural net is done via supervised or unsupervised algorithms. The backpropagation algorithm is an example of the supervised training algorithm. This algorithm was formalized by Rumelhart and McClelland.[10] Supervised learning implies *a priori* knowledge of the desired output. This is akin to a teacher guiding a student along the correct learning path since the teacher is aware of the end result.

For the considered application, the FFBP network comprises four layers as shown in Fig. 37. These layers are classified into the Input, Hidden, and Output layers. Feedforward in FFBP refers to the fact that there are no recurrent loops in the network that provide an active feedback, i.e., the output from a given node does not cycle back immediately to the same node. The interaction between the layers is governed through connections of variable strengths referred to as weights.

In case of supervised learning, the net is repeatedly presented with numerous pairs of input and desired output data. In this specific case, the input refers to the digitized gamma ray and neutron density log values. The output is the desired core porosity. In the beginning, the weights are initialized randomly. The data at the input layer is processed by the neurons and the results are fed-forward to the hidden layer. The hidden layer neurons do similar data processing and pass their results to the output layer. The data at the output layer is then compared against the "desired output" and an error term is calculated. This error term is then backpropagated through the net. This backpropagation of error is carried out by the readjustment of the weights. This process continues till the error term generated at the output layer is minimized within a prespecified tolerance. At this point, the neural net is considered to be trained. Theoretically, within reasonable bounds, the trained net should be capable of predicting porosities from log data that the neural net has never seen before.

Data Collection and Analysis. The as-is data from the old style neutron logs were inappropriate to be used directly as inputs for the neural net. This conclusion was reached because the neutron readings were on different scales. The minimum neutron count varied from 200 to 900, and the maximum neutron count varied from 1200 to 2200. After digitizing the logs by hand, old style neutron and gamma logs were normalized. The neutron logs were normalized by using the minimum and maximum neutron count for each well as shown in the following equation.

$$N_{normalized} = \frac{N_{readings} - N_{min}}{N_{max} - N_{min}} \quad (2)$$

where $N_{readings}$ is the neutron count read on the log, N_{min} and N_{max} are the minimum and maximum neutron count read on the same log.

The gamma ray was scaled by dividing the log values by 100. In order to train the neural network, available information that includes both the logs and measured core porosity must be found. Five wells were selected - two from the Sulimar Queen (wells 1-14 and 5-1) and three wells from the Double L field (wells LL1, LL2, LL3) located a few miles north of the Sulimar Queen. Although the Double L wells are located in another field, we believe that the Queen formation still exhibits the same geological and petrophysical properties as in the Sulimar Queen field. The total number of available core porosities for the 5 wells is 68. The normalized neutron count data for the 5 wells was then plotted as shown in Fig. 38.

An approximate logarithmic trend in the data was observed. The outliers, which have a high neutron count for high porosities, were removed and the remaining dataset was used for calibrating the neural net. The core porosities in the five available wells varied from 5% to 30%. To facilitate the training process, the logarithm of porosity was considered rather than the porosity itself. This transformation reduces the range of data to be handled by the neural net. The new range for the neural network output varies from 1.61 to 3.4 which represents the logarithm of porosity.

In terms of number of inputs at different depths, we considered the tool geometry where the neutron detector is very often located at the top of the tool, and the source at the bottom. Based on this observation, the gamma ray and neutron input to the neural net also included data from immediate readings, 1 ft above and 1.5 ft below the considered depth. Since the log data are available every 0.5 ft, two readings are considered above the current depth and three readings below the current depth. Hence, the total number of inputs for each depth is 12 (6 neutron and 6 gamma readings).

Various studies were also conducted to evaluate the "optimum" time of training of the net. These studies were conducted by varying the prespecified tolerance value referred to earlier. This was done to ensure that the net is not overtrained. Overtraining of the neural net results in deterioration of the generalization capabilities of the net. Overtraining the net is analogous to teaching a child to identify a red ball. The child will identify the red ball correctly, but will fail to recognize that a green ball is a ball.

Once the net was assumed to be optimally trained with 5 wells, it was tested using data from Well 1-3 which was not included in the training. Unfortunately, core data are not available at this well which is located only 200 ft from well 1-16. Since, Well 1-16 is cored and well documented and is very close to Well 1-3 (200 ft away) we assumed that the porosity profile in Well 1-3 is similar to the core porosity observed in Well 1-16 (Fig. 39).

Using the trained neural network, Well 1-3 porosity is estimated (Fig. 40). Because of the wide range of porosity and the lack of a large database for training, the neural network prediction exhibited the following characteristic. The high values of porosities are always and consistently underestimated, while the low values are always overestimated. The neural network prediction are correct around the average porosity. To accommodate for the error introduced for high and low porosities, a correction function which uses the neural net porosity as input and the actual porosity as output is derived. Details concerning the correction function will be described in the future. By using the neural estimated porosity at Well 1-3 and the known porosity available at Well 1-16, the neural net estimated porosity are corrected near the low and high values as shown in Fig. 40. Given the trained neural network and the correction function, 20 pseudo-porosity logs were generated and will be used for reservoir modeling (Fig. 41).

FUTURE RESEARCH PLANS

The four cores listed in Table 4 will be flooded with oil to determine the endpoint for the Amott index I_o and to prepare for a test of spontaneous imbibition of water. Further wettability tests with reservoir cores after cleaning and reaging in crude oil are in the planning stages. The outcrops of Queen sand studied so far have not been judged sufficiently similar to the reservoir core to make comparative studies likely to be meaningful. If more similar rock becomes available, aging studies may be undertaken in initially water-wet outcrop sandstone.

Tests of the oil acidic and basic components are underway. Additional studies of the crude oil's interactions with calcite surfaces may be considered. A single test of adhesion of the crude oil on calcite submerged in reservoir brine has shown strong interaction and many pore surfaces appear to have calcite or dolomite coatings.

More sensitivity analysis will be done on the base case for the SWWTT. The tracer types and tracer reaction kinetics will be studied in the next quarter. We are in the process of investigating the significance of using different relative permeability models that include hysteresis on the design of the tracer test. Other factors such as heterogeneity will also be evaluated on this new base case design.

Future field work includes conducting an aerial survey of the area to determine if there are any more suitable outcrops that have not been located via land surveys, and to examine outcrop architecture and morphology at larger scales than is possible from ground studies. Additional outcrop samples may be collected if it is found necessary for geostatistical description. Petrographic analysis of samples will reveal variations in lithology, depositional and diagenetic history, and relate these variations to changes in petrophysical data. Lithologic comparisons will be made between outcrop and subsurface data, both to see if geostatistical information can be extrapolated into the subsurface reservoir model, and to determine if outcrop samples can be used as reservoir analogs for laboratory studies.

Reservoir modeling work during the coming year will focus on the use of AI and neural networks to enhance our ability to characterize the reservoir from the limited available data. Work on relating porosity and permeability to neutron log response is nearly complete. When that data is available, we will incorporate

it into the reservoir model. Also, interpretation of 2–D geophysical and cross-well tomographic data will be completed and utilized in reservoir modeling.

REFERENCES

1. Morrow, N.R.: "Wettability and Its Effect on Oil Recovery," *JPT* (Dec. 1990) 1476-1484.

2. Ma, S., Morrow, N.R., Zhou, X., and Zhang, X.: "Characterization of Wettability from Spontaneous Imbibition Measurements," paper CIM 94-47 presented at the 1994 Petr. Soc. of CIM Ann. Tech. Meeting and AOSTRA 1994 Ann. Tech. Conf., Calgary, June 12-15.

3. Jadhunandan, P. and Morrow, N.R.: "Effect of Wettability on Waterflood Recovery for Crude Oil/Brine/Rock Systems," *SPERE* (1995) **10**, No. 1, 40-46.

4. Liu, Y. and Buckley, J.S.: "Evolution of Wetting Alteration by Adsorption from Crude Oil," SPE 28970 presented at the 1995 International Symposium on Oilfield Chemistry, San Antonio, Feb. 14-17.

5. Wilson, J.L., *Carbonate Facies in Geologic History*: New York, Springer-Verlag, 471, 1975.

6. Mazzullo, S. and Hedrick, C.: "Road Log, Day One - Back-Reef Facies," *in* B.K. Cunningham, C.L. Hedrick, and C. Beard (eds.), *Permian Carbonate/Clastic Sedimentology, Guadalupe Mountains: Analogs for Shelf and Basin Reservoirs.* Annual Field Trip Guidebook, 1985: Permian Basin Section, SEPM Publ. 85-24.

7. Sarg, J.F.: "Locality Guides, Sops VI, VII, and VIII, Rocky Arroyo," *in* L.C. Pray,and M.C. Esteban (eds.), *Upper Guadalupian Facies, Permian Reef Complex, Guadalupe Mountains, New Mexico and Texas, Vol. 2, Road Logs and Locality Guides:* Permian Basin Section , SEPM, Publ. 77-16, 1977.

8. Cowen, T.M., 1988, Preliminary Geologic Reservoir Study, Sulimar Queen Field, Chaves Co., New Mexico.

9. Ouenes, A. *et al.*: ``A New Approach Combining Neural Networks and Simulated Annealing for Solving Petroleum Inverse Problems," paper presented at the 1994 European Conference on the Mathematics of Oil Recovery, Roros, Norway, June 7-10.

10. Rumelhart, D.E. and McClelland, J.L.: *Parallel Distributed Processing, Volume 1: Foundations*, MIT Press, Cambridge, MA (1986).

Table 1. Cores Used in Centrifuge Study.

Depth	1996.2	1998.1
ϕ (%)	24.49	23.14
L (cm)	4.985	4.953
D (cm)	3.719	3.716
K_{N2} (md)	61.8	38
$K_{w,i}$ (md)	6.28	1.22
$K_{o,Swi}$ (md)	34	21
$K_{w,Sor}$ (md)	18	10
$K_{o,Swi}$ (md)	52	23
I_w	0.002	0.193
I_o	0.503	0.576
I_{AH}	-0.501	-0.383
I_{USBM}	-0.35	-0.32

Table 2. Synthetic Reservoir Brine.

Salts	mg/L
$NaHCO_3$	282
Na_2SO_4	4,303
$CaCl_2 \cdot 6H_2O$	7,776
$MgCl_2 \cdot 6H_2O$	74,612
NaCl	262,314

Table 3. Sequence of Experiments.

Step	Experiment	displacing phase
1	P_c	oil
2	P_c	water
3	P_c	oil
4	k_r	water
5	k_r	oil
6	P_c	gas
7	k_r	gas
8	cleaning	1) Dean-Stark 2) flowing toluene, methanol, and THF
9	K_{N2},ϕ	

Table 4. Cores Used in Spontaneous Imbibition Experiments.

Core ID	SQ-1	SQ-2	SQ-3	SQ-4
Depth (ft)	2002.0 to .4	1995.6	2002.5	2007.4 to .6
Preserved?	yes	no	no	yes
L (cm)	6.77	5.78	3.18	5.96
D (cm)	3.565	3.59	3.59	3.59
$K_{w,i}$ (md)	< 0.1	39.7	2.0	0.34

Table 5. Adsorption Tests with Sulimar Queen Crude Oil on Glass Surfaces Pretreated with Various Brines.

Brine	pH	T_{aging} (°C)	water/oil contact angles (deg)		
			θ_a	θ_r	t_{aging} (days)
0.01 *M* NaCl	4	25	76	46	29
	6		48	29	26
	8		54	34	21
1.0 *M* NaCl	4		40	24	29
	6		46	27	26
	8		30	24	21
0.01 *M* NaCl	4	80	79	34	20
	6		25	18	20
	8		29	20	22
1.0 *M* NaCl	4		81	28	20
	6		25	19	21
	8		80	46	22
4.25 *M* NaCl	4	25	88	43	25
	6		66	33	25
5.0 *M* NaCl	8	25	33	24	25
Reservoir brine (Table 2)	6.1	32	32	25	20
3/4 strength reservoir brine	6.3	25	67	37	25

Table 6. Adsorption from Sulimar Queen Crude Oil onto Dry Glass Surfaces.

T_{aging} (°C)	t_{aging} (days)	θ_a (deg)	θ_r (deg)
25	31	61	35
80	5		
25	0.25	62	38
	2	119	67
	5	136	72
	9	101	55
	14	134	65
	20	129	64
	22	145	180

Table 7. Parameters used in the four layer model.

Layer	*Depth* (ft)	*Thickness* (ft)	*Porosity* (%)	*Permeability* (md)		*Initial Saturations* (%)	
1	1995-1996	1	15.4	$k_x = 74$	$k_z = 7.4$	$S_w = 65$	$S_o = 35$
2	1996-2003	7	20.8	$k_x = 51$	$k_z = 4.3$	$S_w = 61$	$S_o = 39$
3	2003-2004	1	20.1	$k_x = 85$	$k_z = 8.5$	$S_w = 64$	$S_o = 36$
4	2004-2005	1	9.4	$k_x = 41$	$k_z = 4.1$	$S_w = 52$	$S_o = 48$

Table 8. Tracer properties used in the base case simulation.

Tracer	*Partition coef.* (mg/L/mg/L)	*Reaction constant* (day^{-1})	*Density* (g/cm^3)	*Molecular Weight*
Ethyl formate (EtFr)	4.03	0.1351	0.917	74.08
Propyl formate (PrFr)	10.25	0.12	0.906	88.12
Methanol (MeOH)	0.0	-	0.791	32.04
Ethanol (EtOH)	0.0	-	0.789	46.07
Octanol (OcOH)	°	-	0.826	130.23
Normal propyl (NPA)	0.0	-	0.786	60.10

Table 9. Injection time and tracer slug size used in the simulation.

Injected	*Volume* (bbl)	*Injection rate* (bbl/day)	*Injection time* (day)	*Tracers*
Water slug with tracers	30	15.5	1.94	MeOH and EtFr
Water slug	30	15.5	1.94	MeOH
Oil slug with tracers	30	15.5	1.94	OcOH and PrFr
Oil slug	50	15.5	3.23	OcOH

Table 10. Amount of tracers used.

Tracer	*Density* (g/cm^3)	*Inj. concentr.* (vol%)	*Volume* (L)	*Weight* (kg)
Ethyl formate (EtFr)	0.917	4	190.8	174.9
Propyl formate (PrFr)	0.906	2	95.4	86.4
Methanol (MeOH)	0.791	0.5	47.7	37.7
Octanol (OcOH)	0.826	0.5	63.6	52.5

Table 11. Input parameters used in the base case SWWTT simulation.

Depth	1995-2005 ft
Pay thickness	10 ft
Radius of reservoir (31 gridblock)	155 ft.
Reservoir pressure	719 psia
Grain density	2.65 g/cm^3
Formation volume factor (oil)	1.15 bbl/STB
Formation volume factor (water)	1.005 bbl/STB
Oil density at 86°F	0.834 g/cm^3
Brine density at 86°F	1.141 g/cm^3
TDS in the brine	308 g/L
Oil viscosity at 86°F	7.67 cp
Brine viscosity at 86°F	1.51 cp
Interfacial tension of brine-oil	21 dyne/cm
Rock compressibility	3.1×10^{-6} psi^{-1}
Oil compressibility	1.4×10^{-5} psi^{-1}
Water compressibility	3.0×10^{-6} psi^{-1}
Aqueous Longitudinal dispersivity	0.1 ft
Aqueous Transverse dispersivity	0.003 ft
Oleic Longitudinal dispersivity	0.1 ft
Oleic Transverse dispersivity	0.003 ft
Reservoir temperature	86°F
Skin factor	2.6
Production rate	44.88 ft^3/day (=8.0 bbl/day)
Injection rate	86.96 ft^3/day (=15.5 bbl/day)

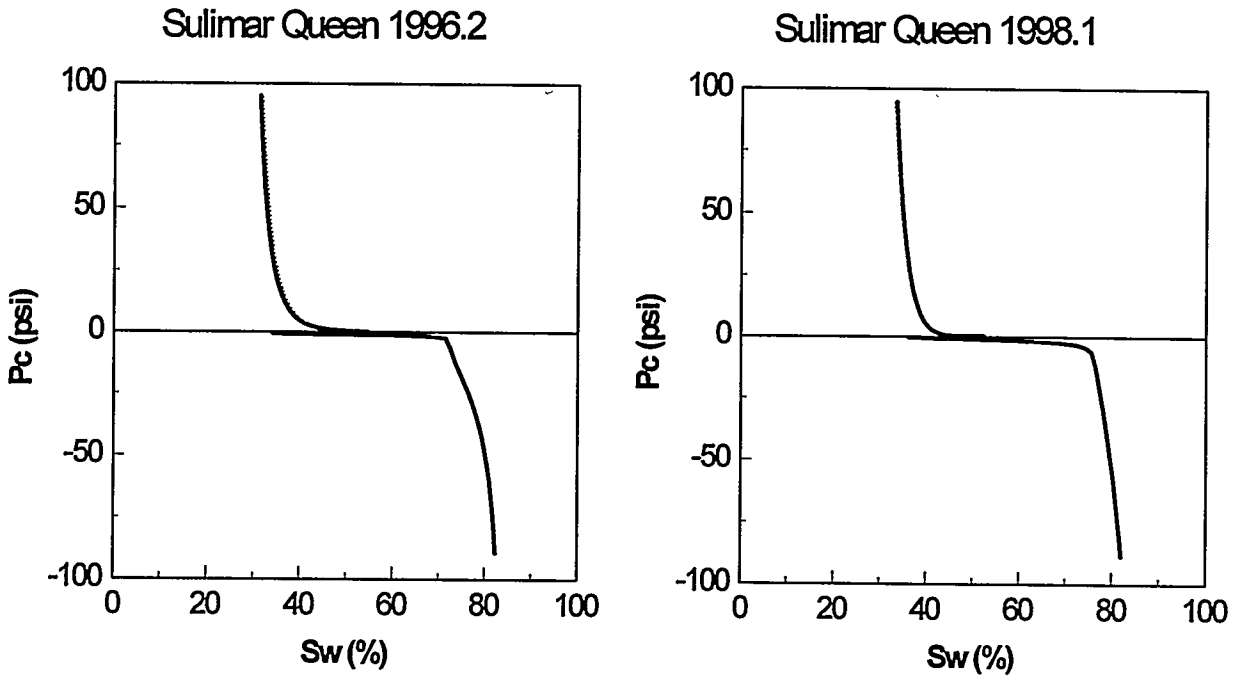

Figure 1. Capillary pressure curves for Sulimar Queen preserved cores from depths of 1996.2 and 1998.1 ft.

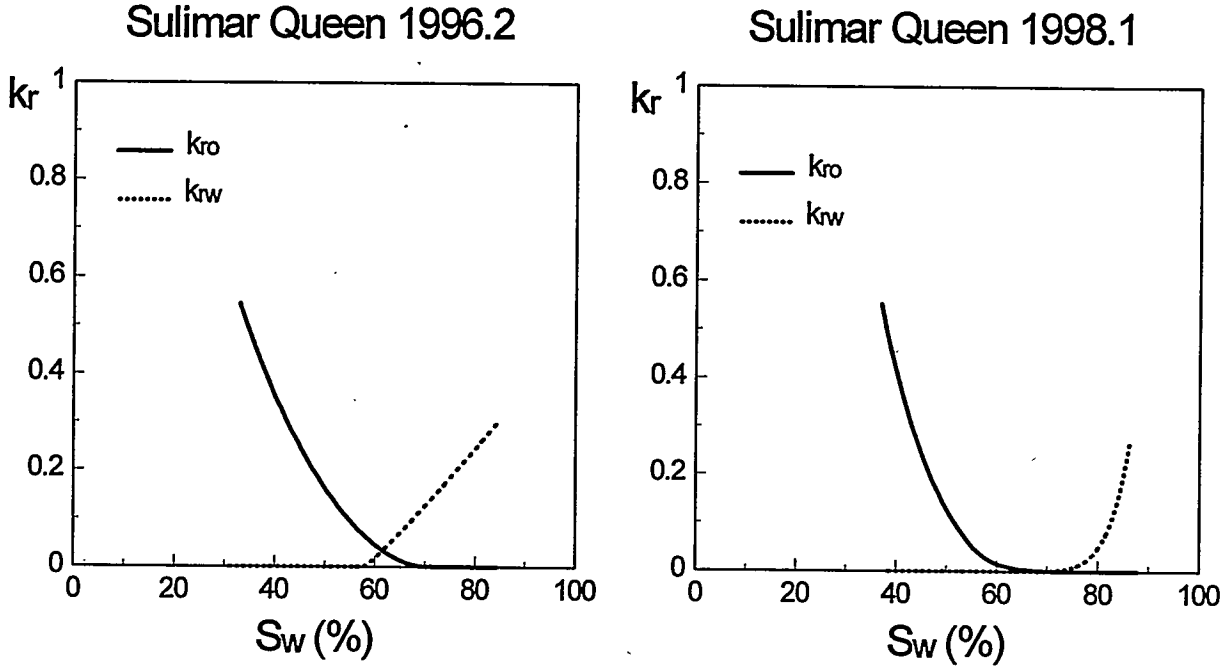

Figure 2. Relative permeability curves for Sulimar Queen preserved cores from depths of 1996.2 and 1998.1 ft (linear scale).

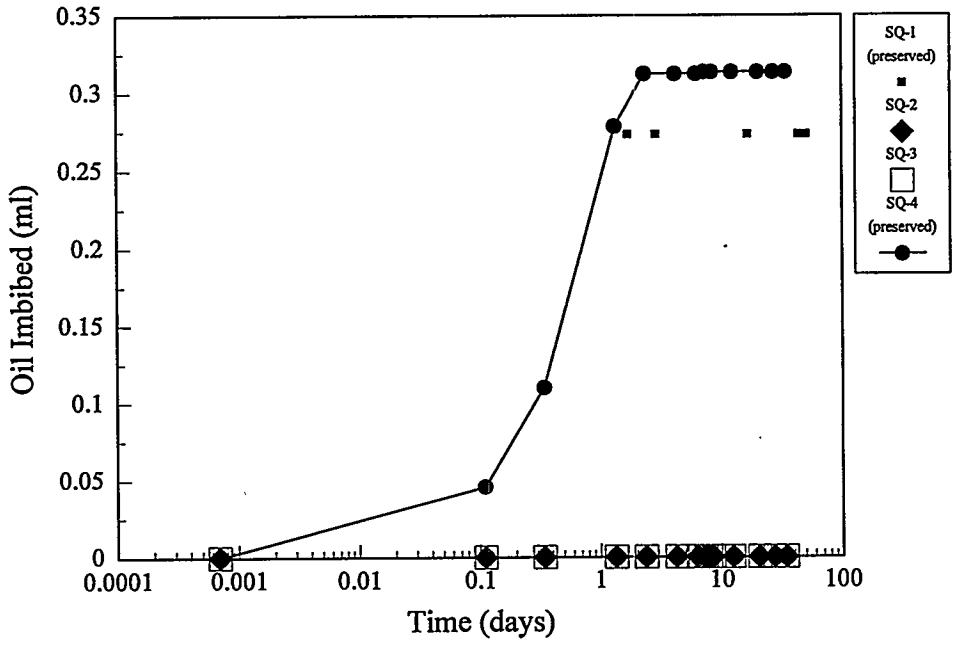

Figure 3. Spontaneous imbibition of oil into Sulimar Queen preserved and unpreserved cores.

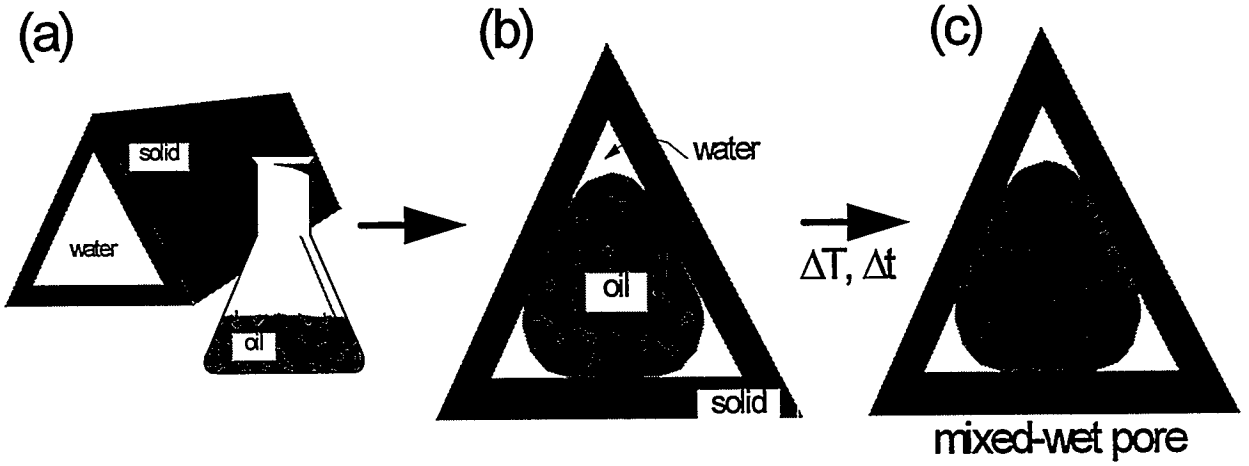

Figure 4. Schematic representation of generation of mixed-wetting in COBR ensemble: (a) triangular pore is water-filled and water-wet; oil contains interfacially active components, (b) oil enters pore as nonwetting phase, (c) after some time (Δt) at elevated temperature (ΔT), components of the oil are adsorbed on portions of the solid surface, changing its wettability.

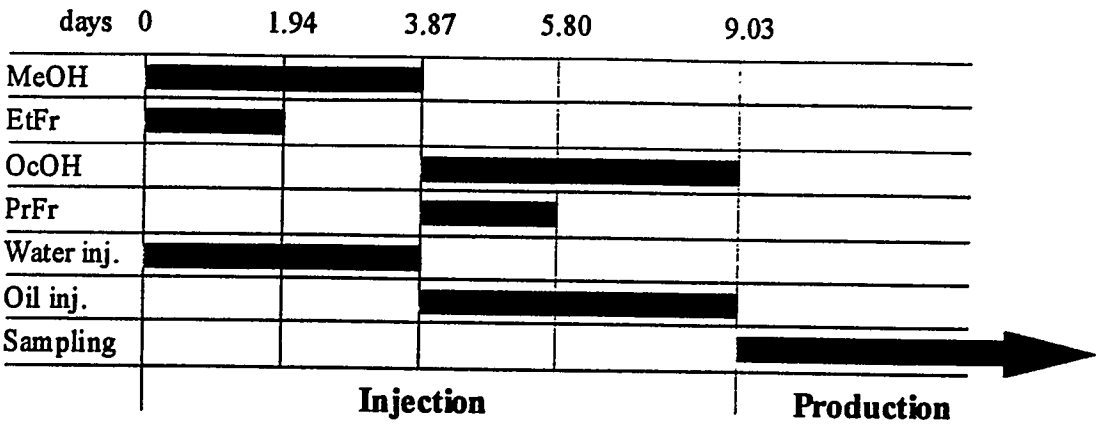

Fig. 5. Timeline for the single well wettability tracer test.

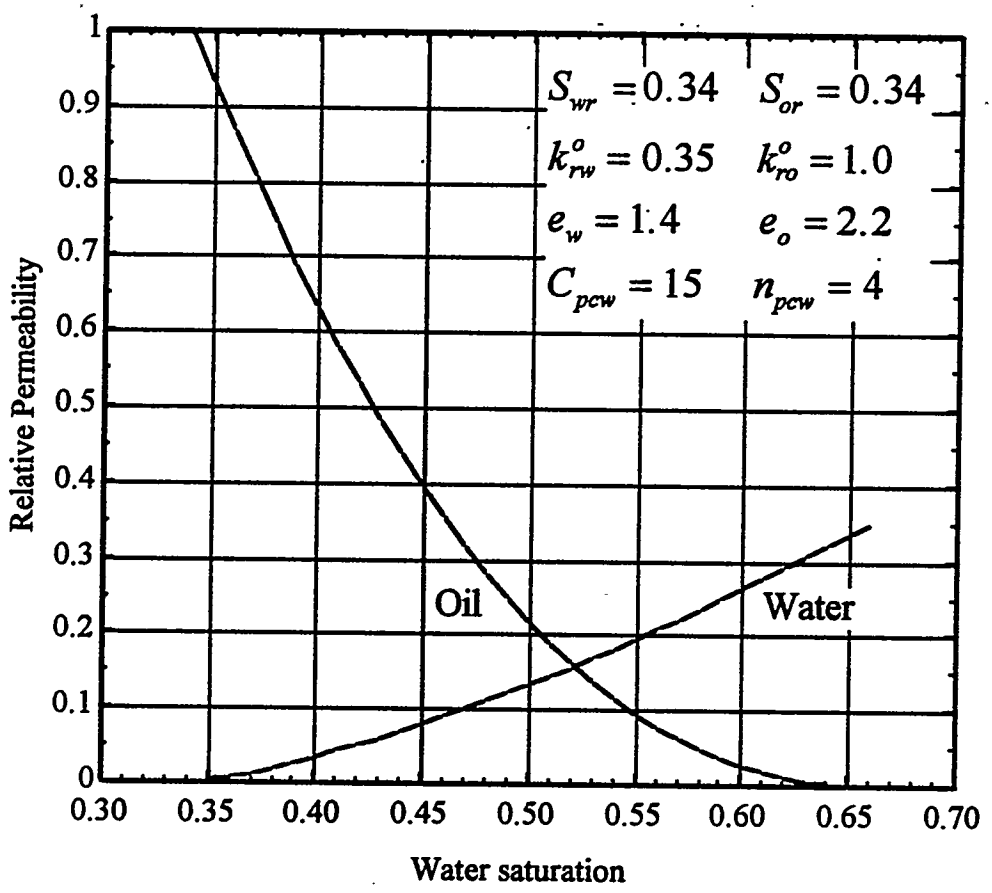

Fig. 6. Relative permeability curves for the weakly water wet case.

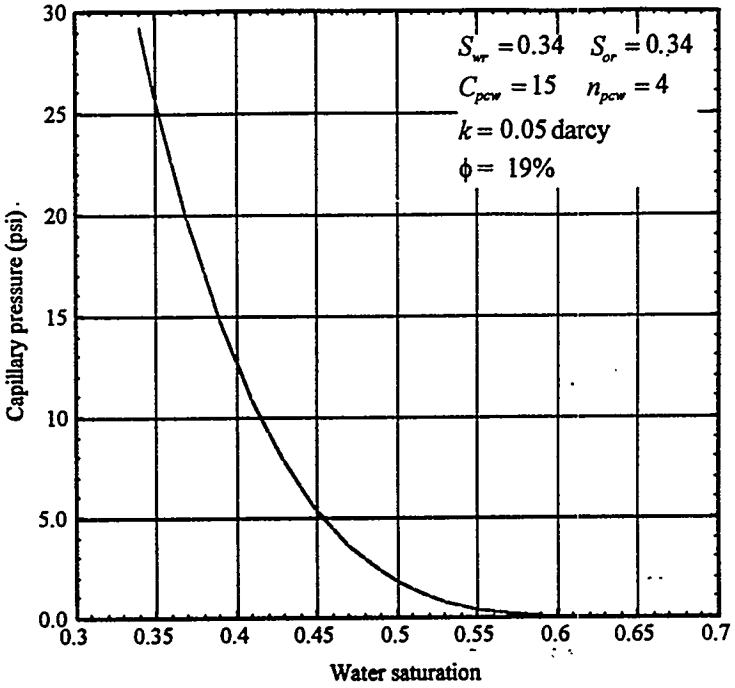

Fig. 7. Capillary pressure curve used for the weakly water wet media.

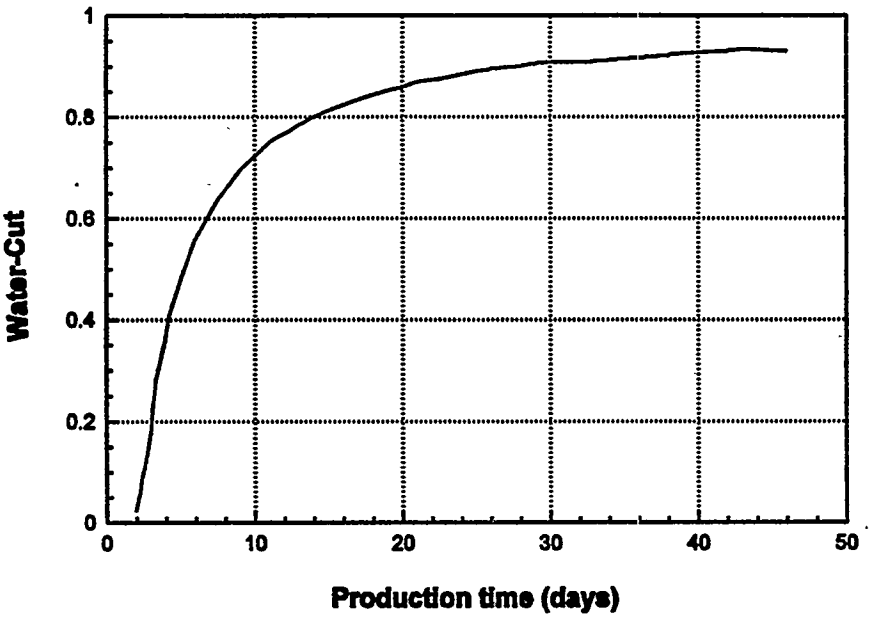

Fig. 8. Water-cut history for the base case SWWTT simulation.

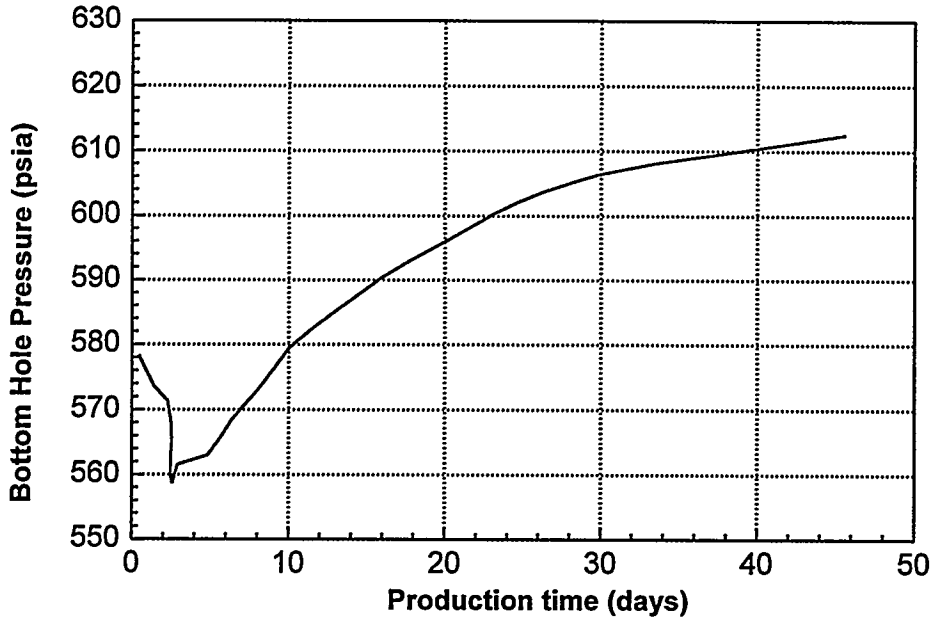

Fig. 9. Bottom hole pressure for the base case SWWTT simulation.

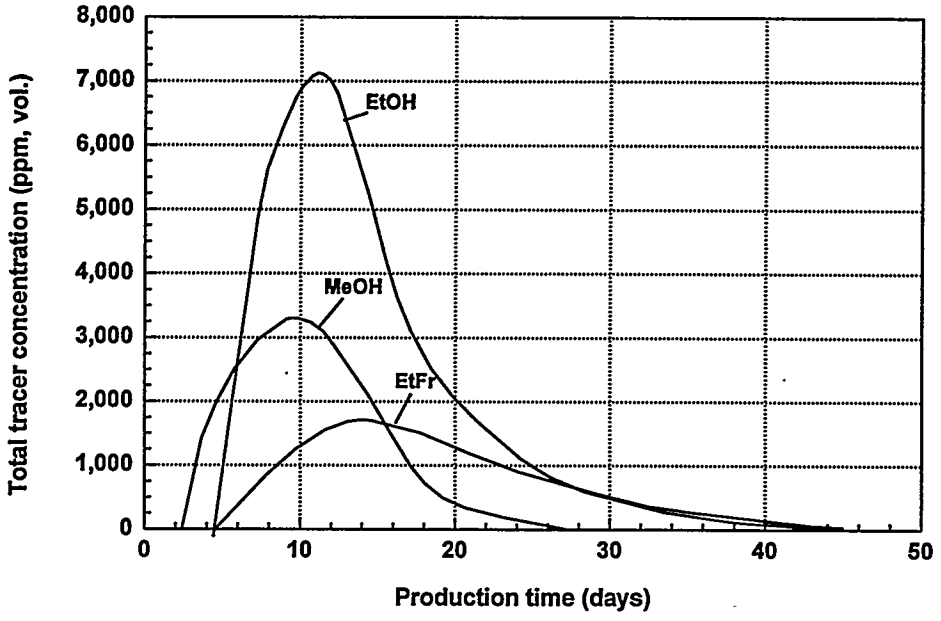

Fig. 10. Response curves for tracers used in the water-slug.

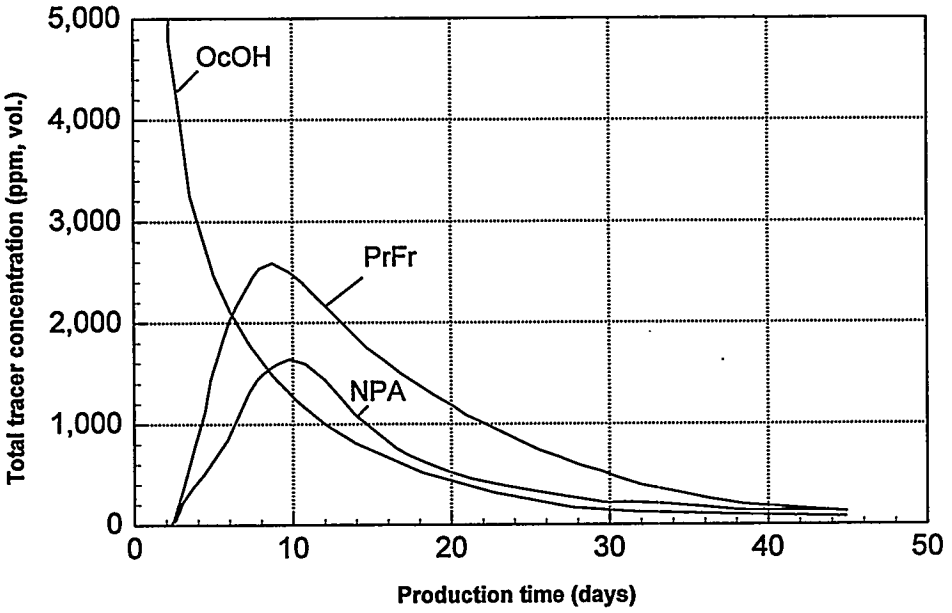

Fig. 11. Response curves for tracers used in the oil-slug.

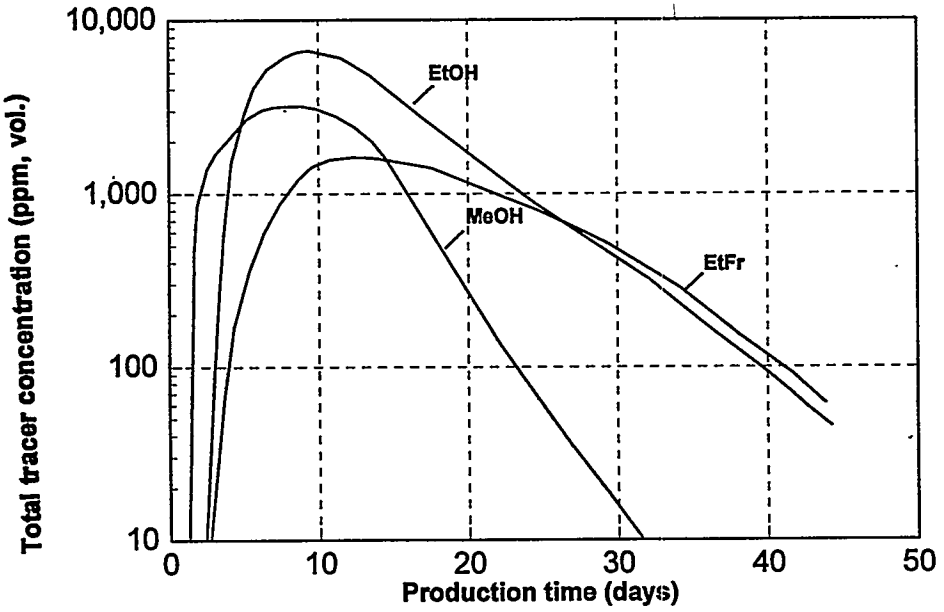

Fig. 12. Water-slug tracers. Plotted above 10 ppm, which is the detection limit.

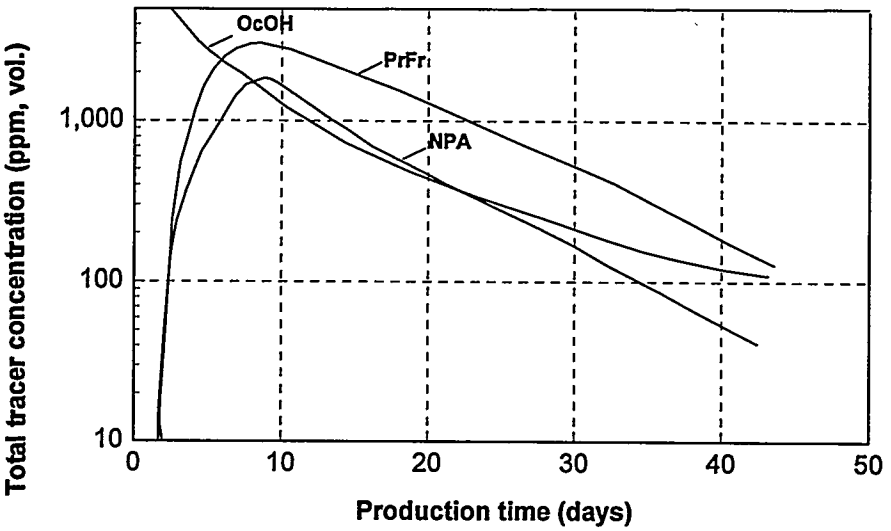

Fig. 13. Oil-slug tracers. Plotted above 10 ppm which is the detection limit.

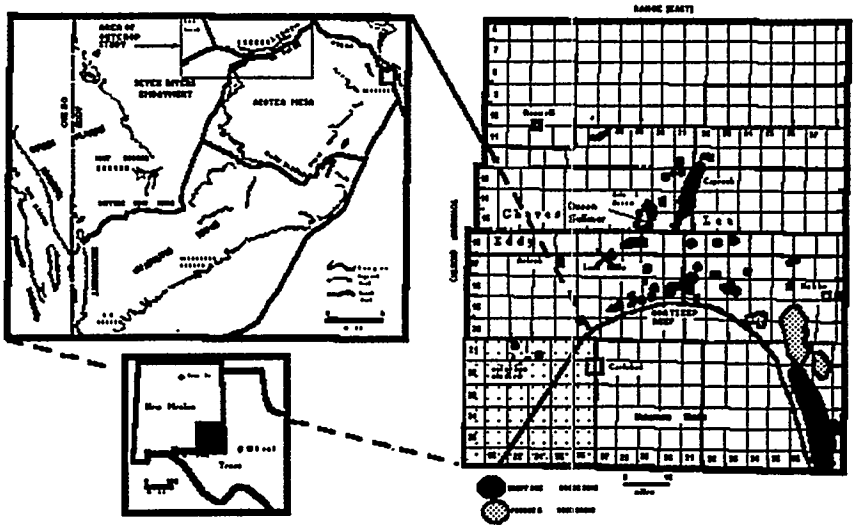

Figure 14. Map of southeast New Mexico, showing location of outcrops, Sulimar Queen field, and position of the Goat Seep shelf margin during time of Queen deposition.

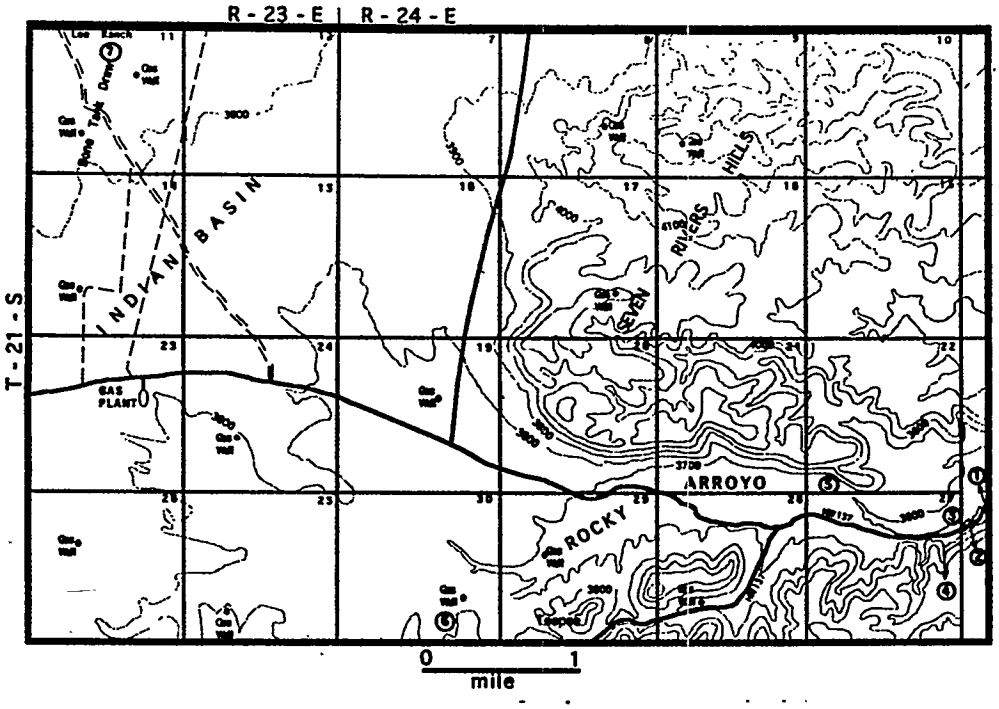

Figure 15. Location of various measured sections described in this study. Circled number indicates the number of the section.

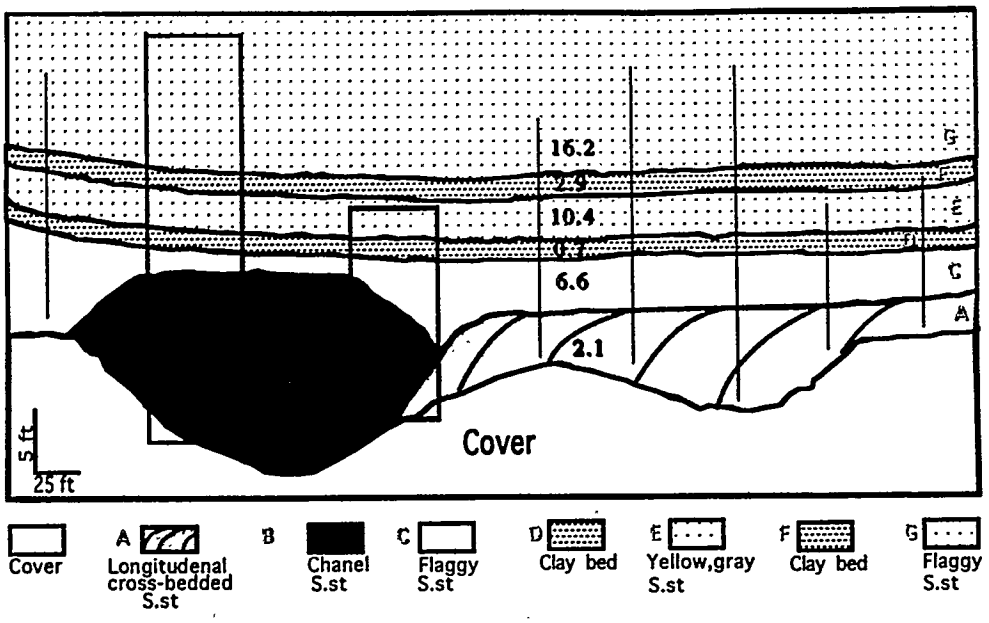

Figure 16. (a) Schematic description of measured Section 2, showing various units and sedimentary structures. (b) Diagram of variation of permeability and grain size in Section 2.

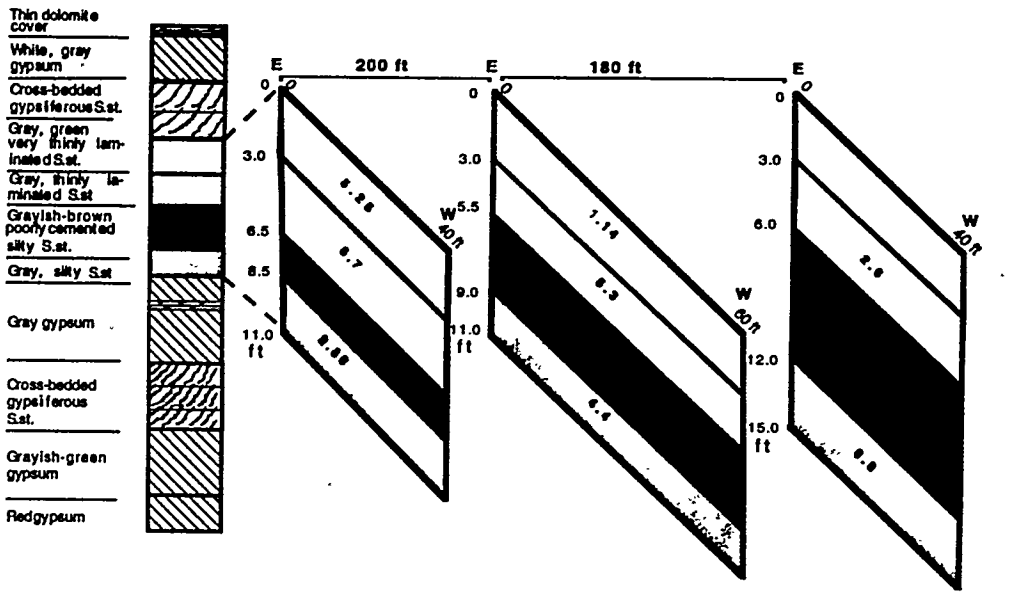

Figure 17. Schematic measured section description of Bone Tank Draw section (Section 7).

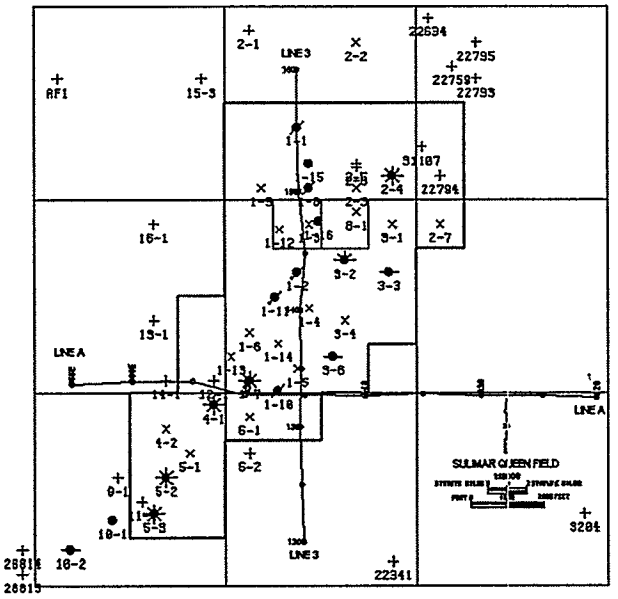

Fig. 18. Basemap of Sulimar Queen field, showing locations of wells and seismic lines.

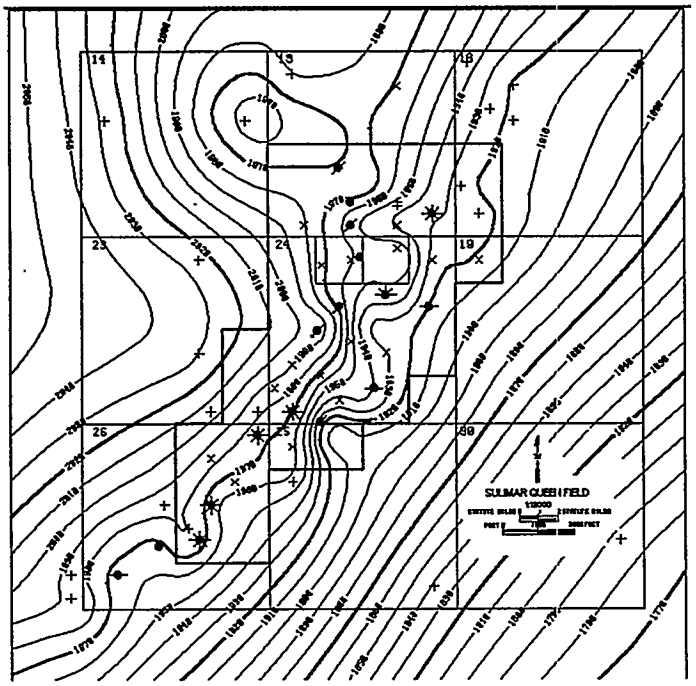

Fig. 19. Structural contour map made on top of Shattuck sand. Elevations are in feet above sea level.

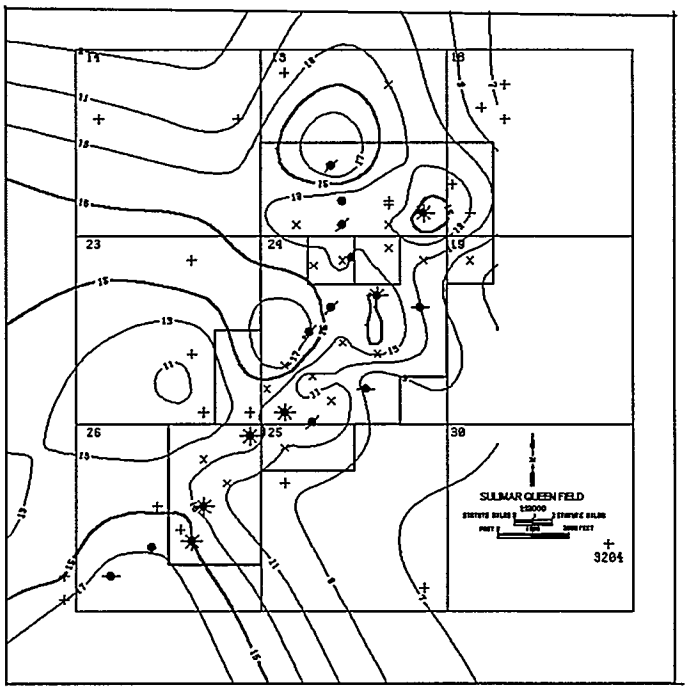

Fig. 20.Gross sand thickness map for the Shattuck sand.

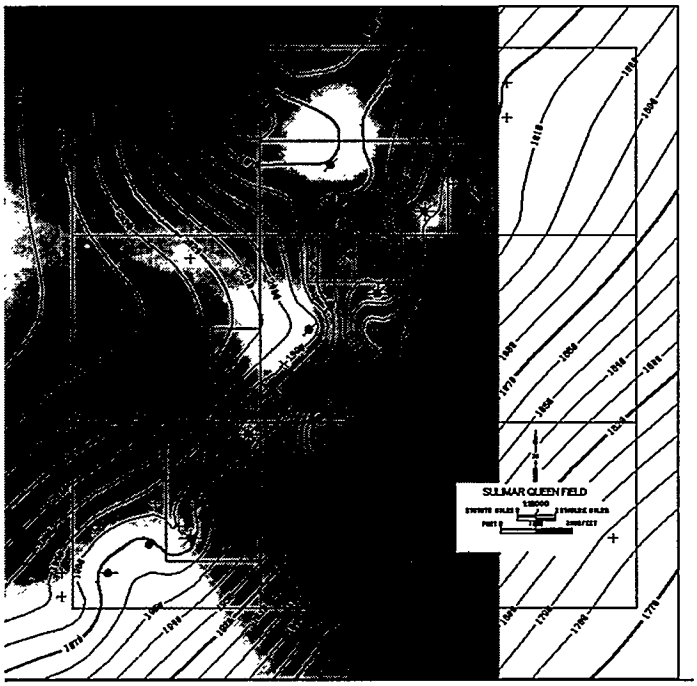

Fig. 21. Overlay of structure contour map and sand thickness map. Lightest areas are structural highs, darker areas are lower.

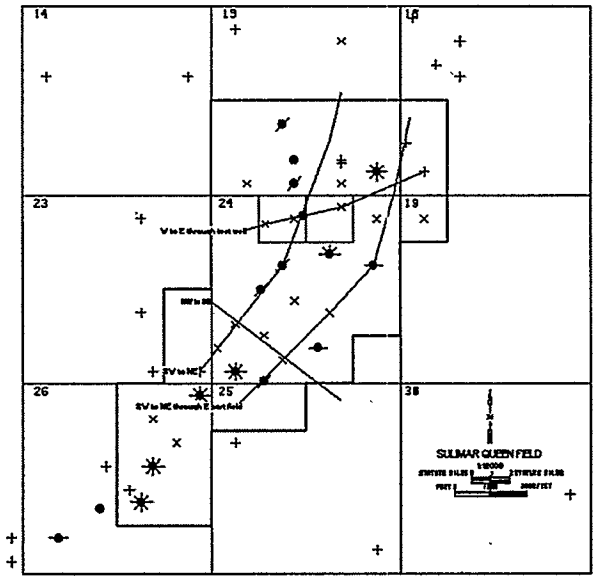

Fig. 22. Base map of Sulimar Queen field showing locations of cross-sections shown in Figs. 23 and 24.

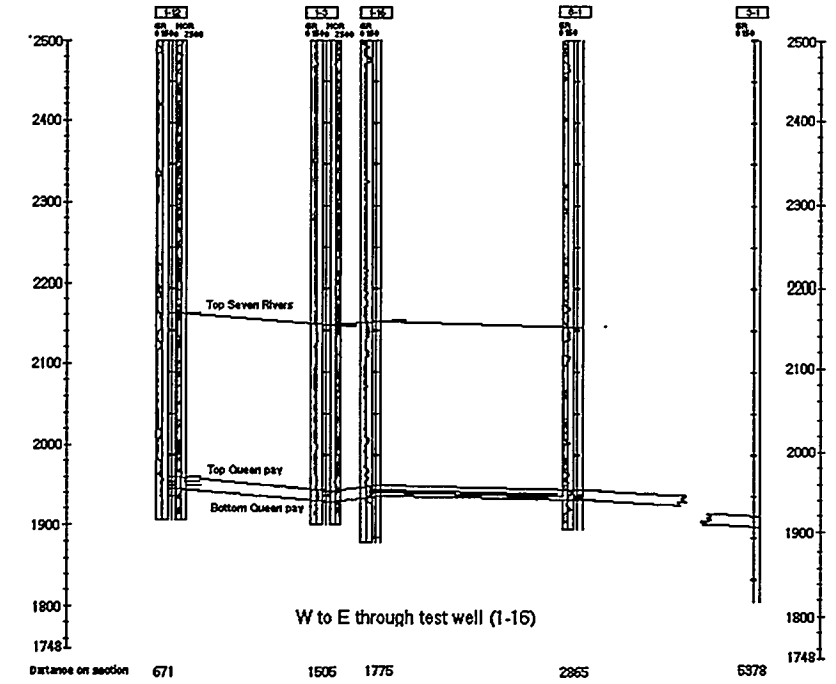

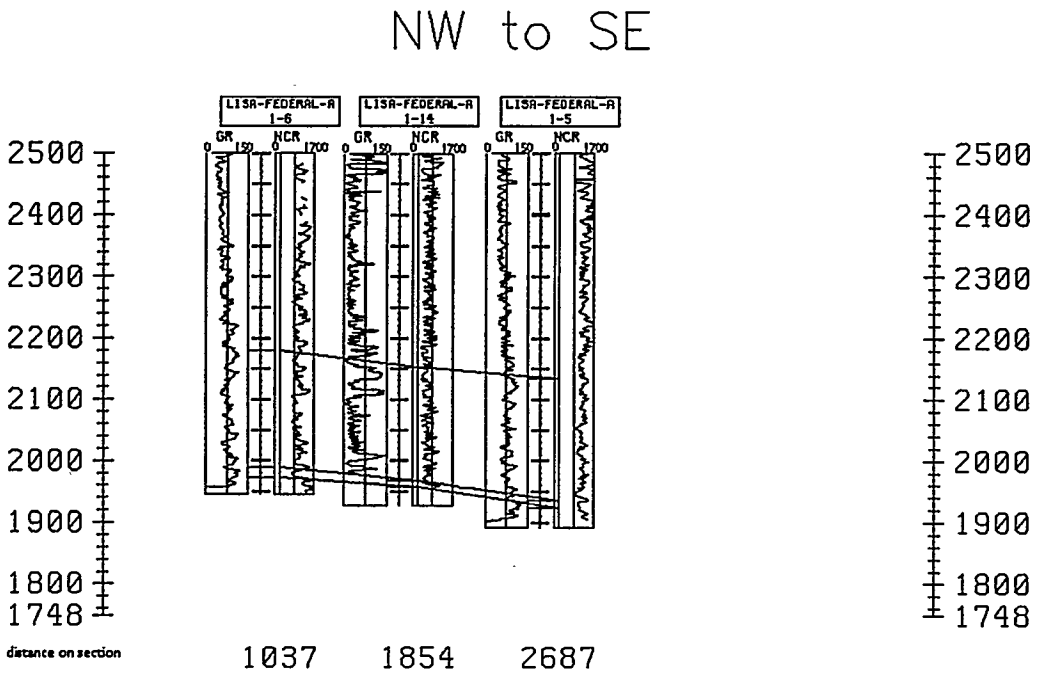

Fig. 23. Cross-sections from west to east across the Sulimar Queen field, showing general regional dip from west to east across the field. The two wells in the center of the top section (1-3 and 1-16) are the two wells used in the cross-well tomography tests.

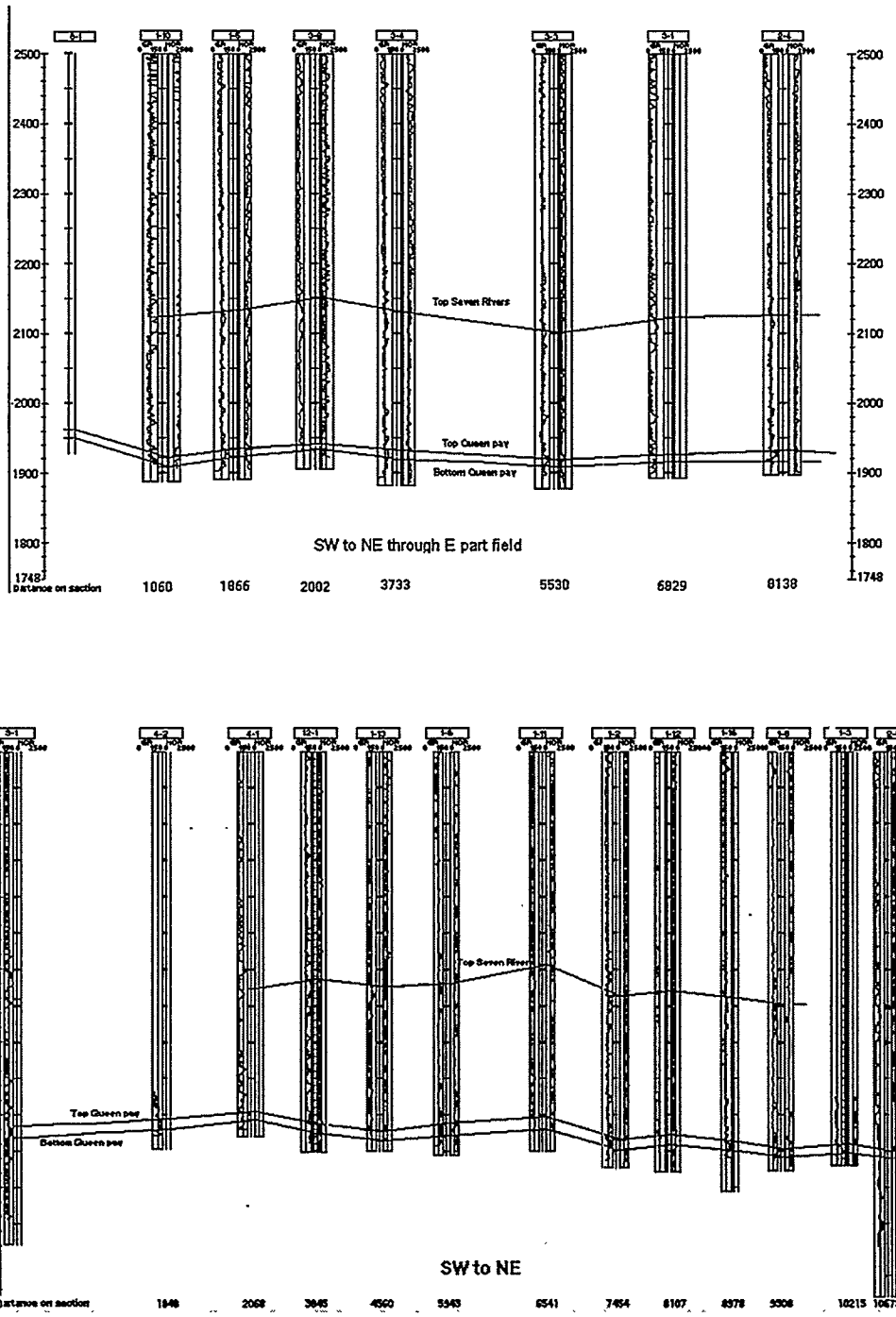

Fig. 24. Cross sections from southwest to northeast across the Sulimar Queen field. Both sections show a general thickening of the Queen towards the center of the field, as well as the presence of the structural highs that trend approximately perpendicular to regional strike.

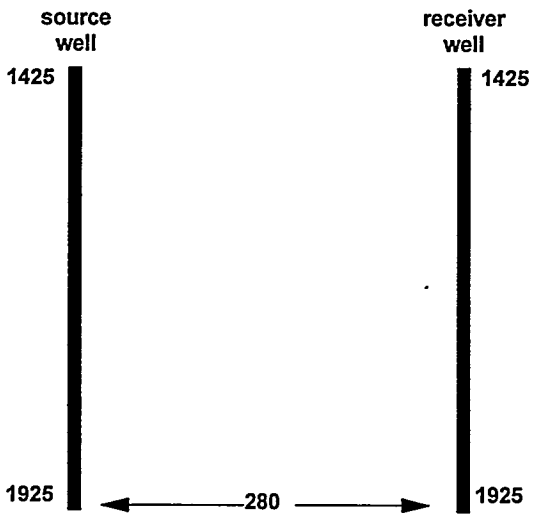

Fig. 25. Crosswell Survey Geometry.

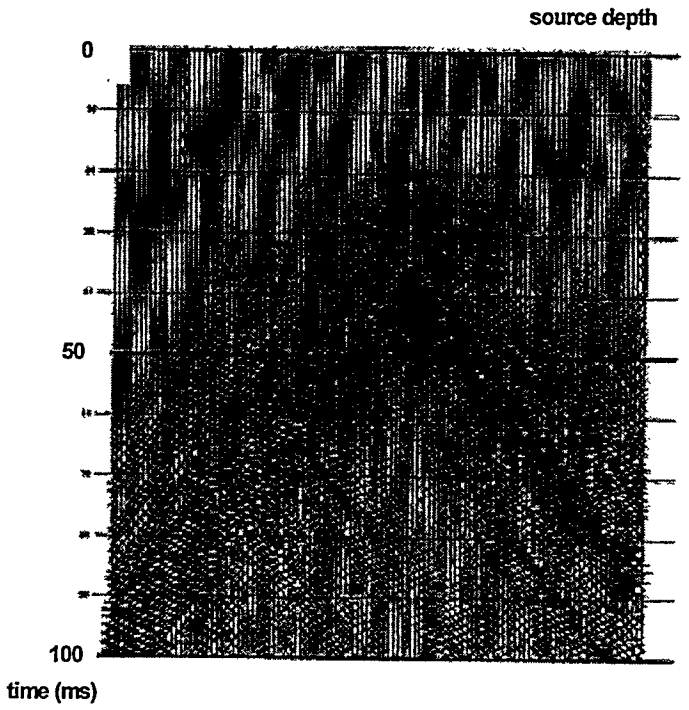

Fig. 26. Common Receiver Gatherer of Raw Data after Correlation with Source Sweep.

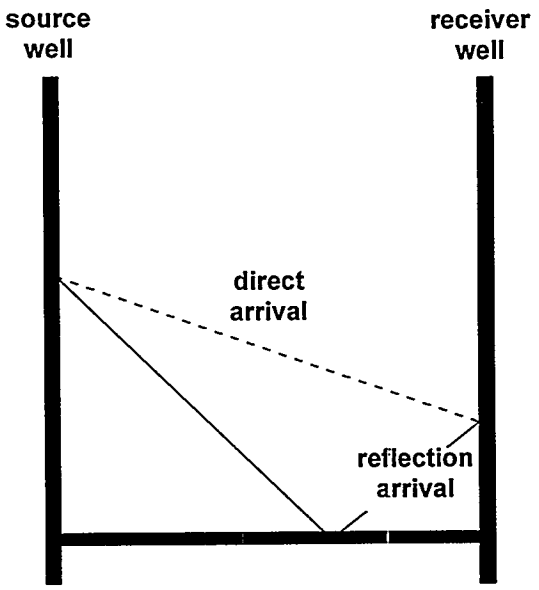

Fig. 27. Raypath Geometry of Direct and Reflected Arrivals

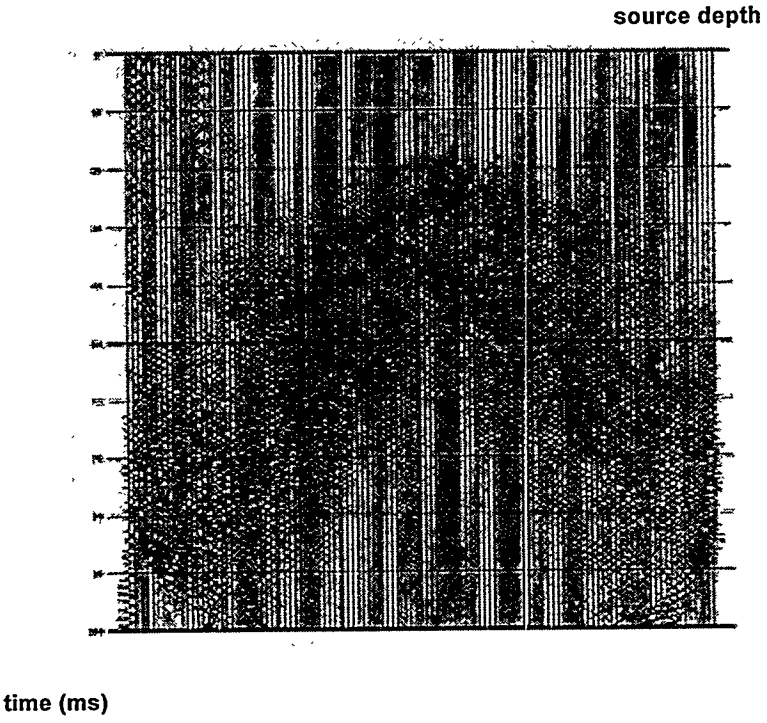

Fig. 28. Common Receiver Gatherer after Tube Wave Removal.

Fig. 29. Modulus of the Analytical Signal of the Common Offset Gather (Offset = 0 Ft).

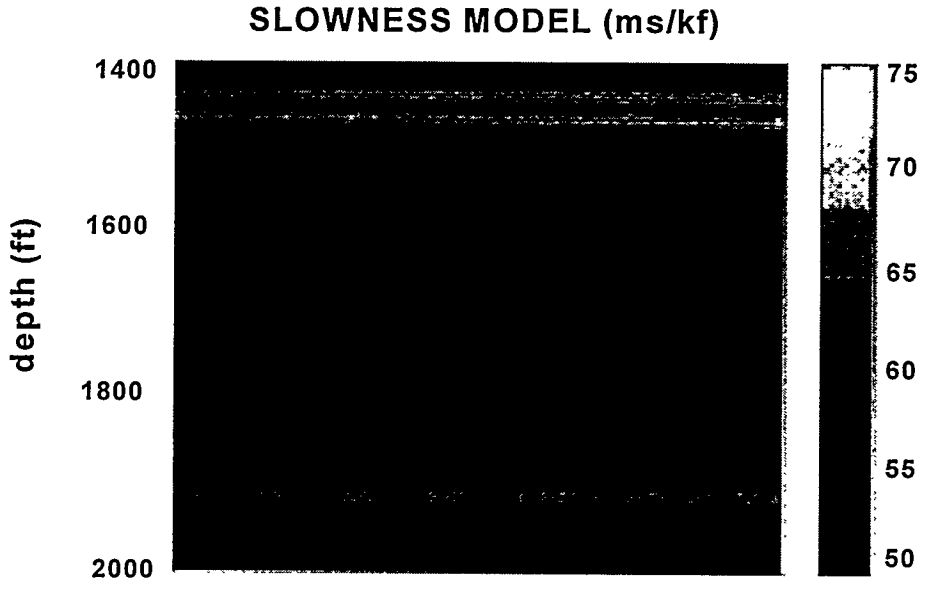

Fig. 30. Velocity Model from Smoothed Sonic Log

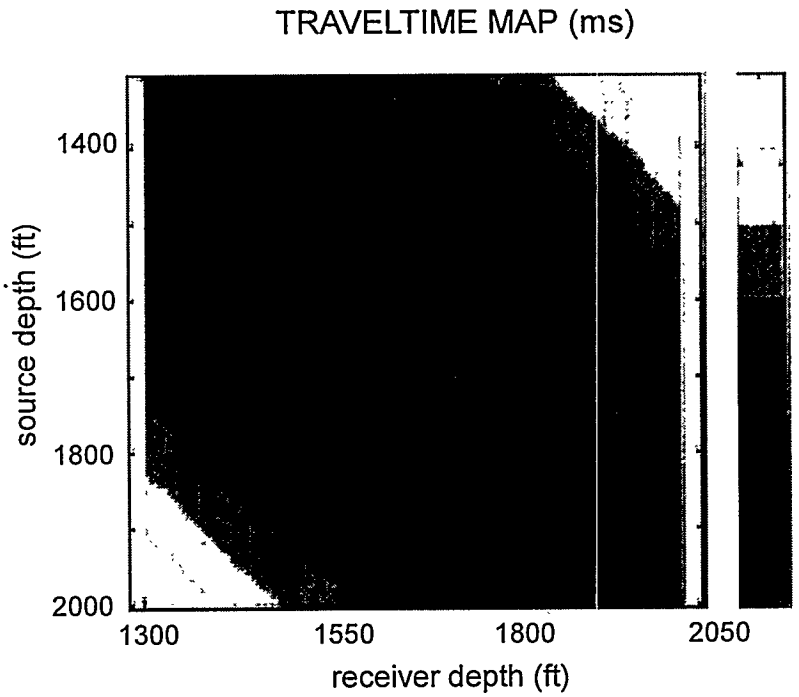

Fig. 31 Sonic Log Based Synthetic Traveltimes.

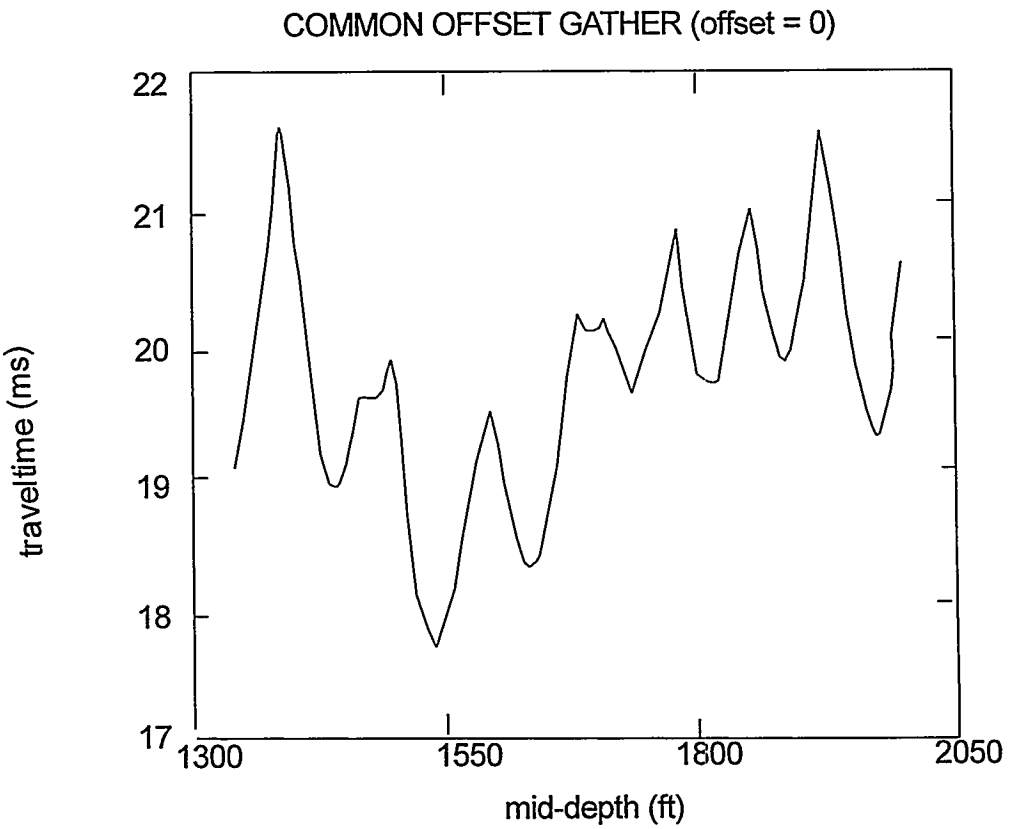

Fig. 32 Zero Offset Gather Synthetic Traveltimes.

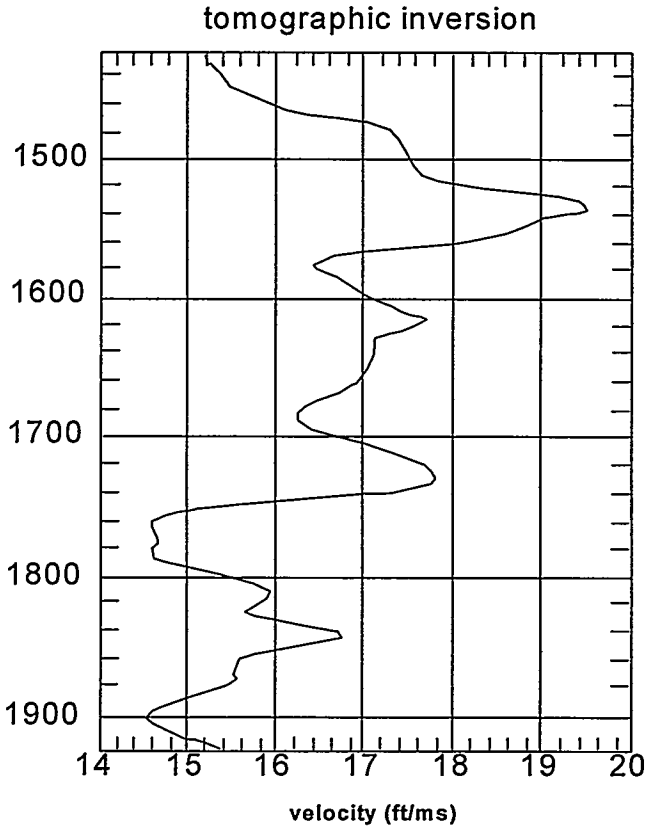

Fig. 33 Tomographic velocity image

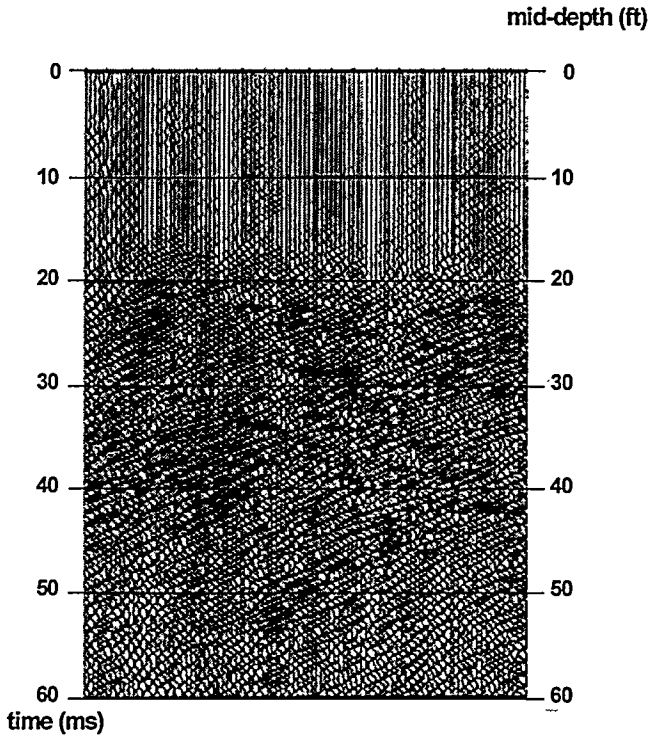

Fig. 34 Common Offset Gather after Wavefield Separation.

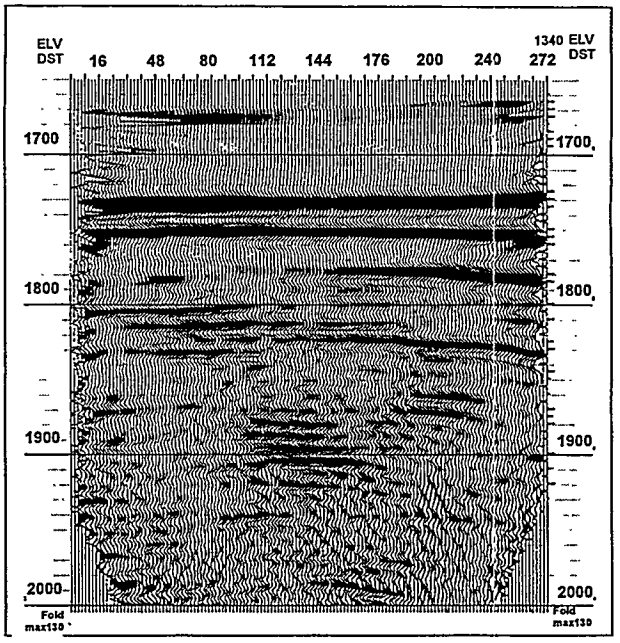

Fig. 35 Reflection Image Stack over a Limited Range of Common Midpoint Gathers.

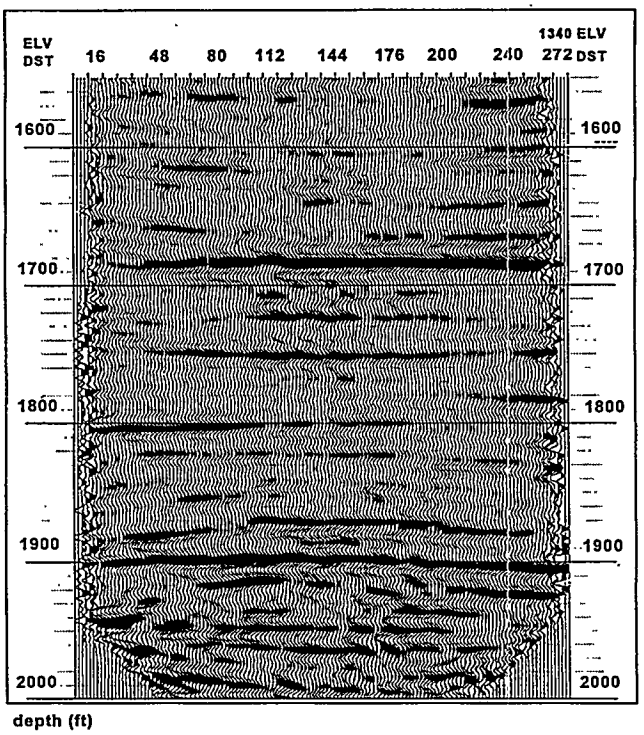

Fig. 36 Reflection Image Stack over the Optimal Incidence Angle Range.

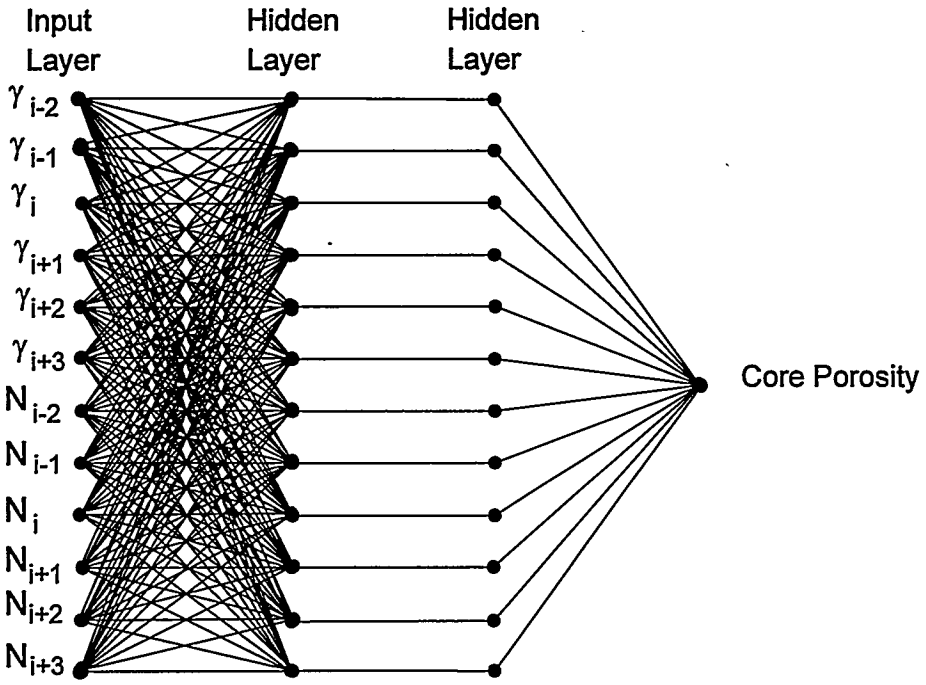

Fig. 37. The Feedforward Backpropagation Neural Net.

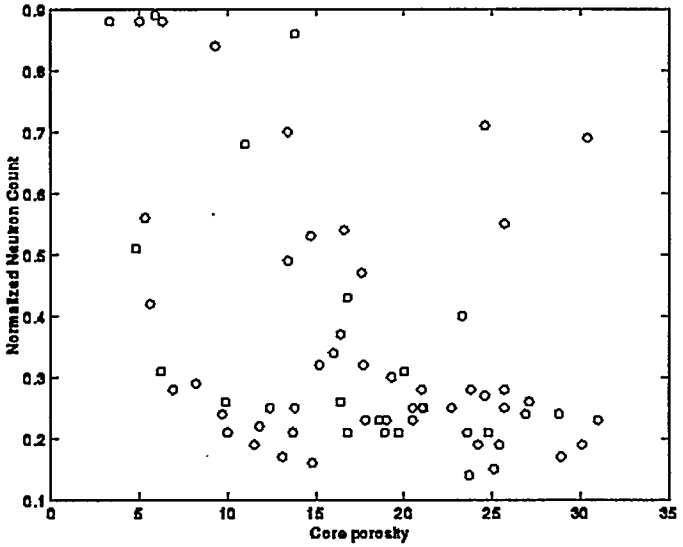

Fig. 38. Plot of the Normalized Neutron Count Data for the Five Wells.

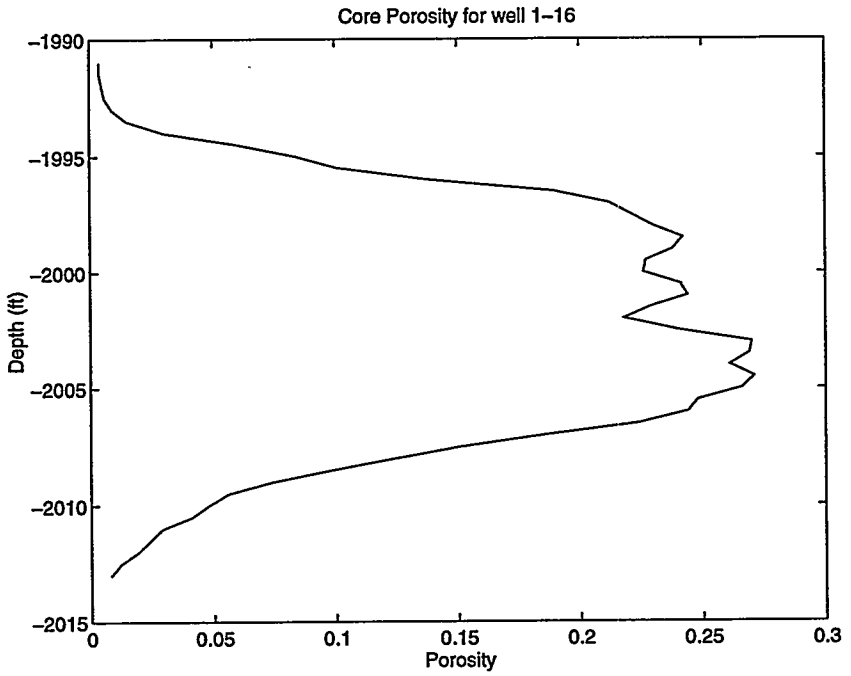

Fig. 39. Core Porosity Observed in Well 1-16.

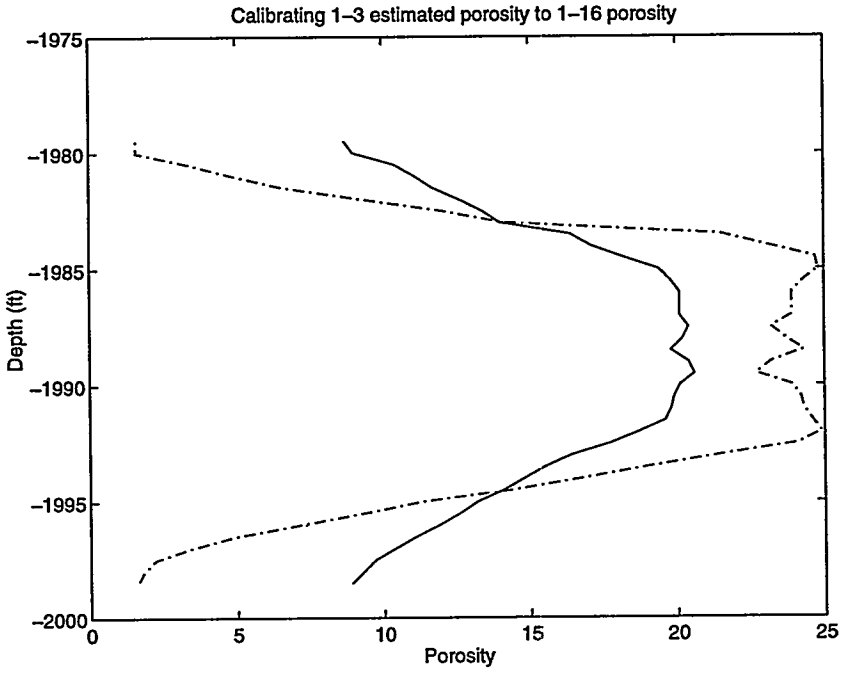

Fig. 40. Correction of Neural Net Estimated Porosity near the Low and High Values.

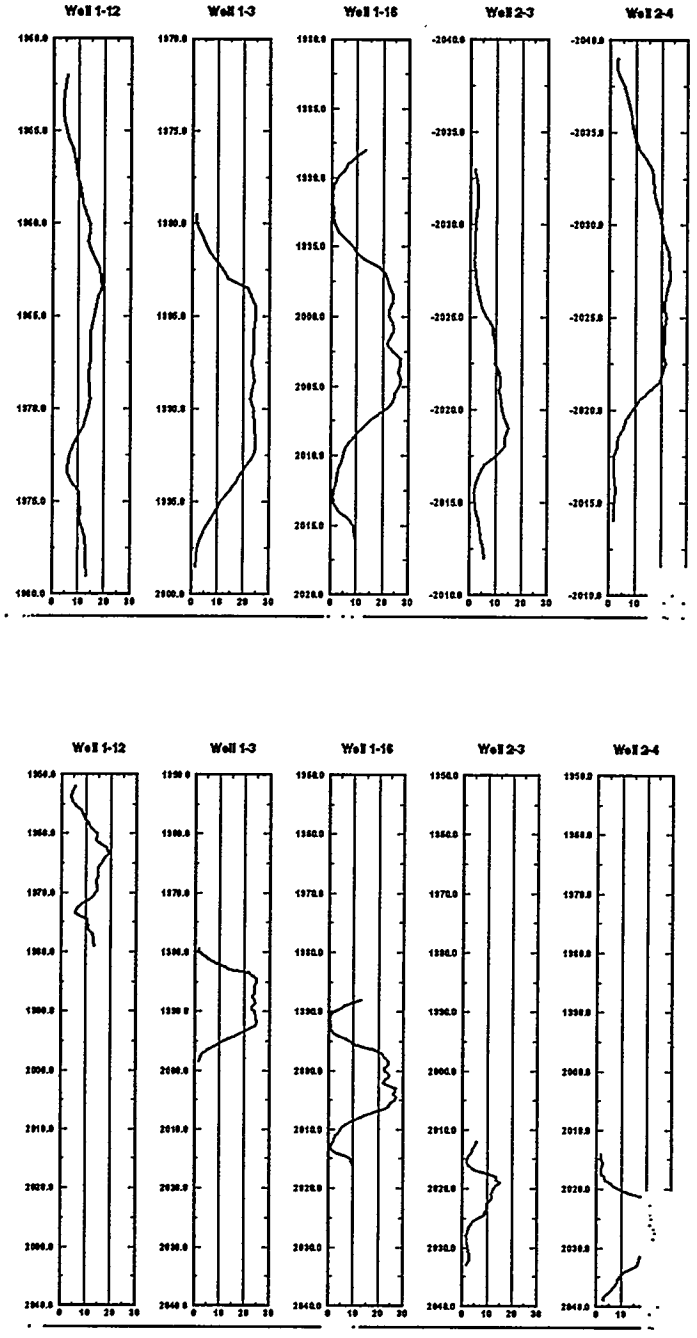

Fig. 41. Cross Section Generated with Pseudo-porosity Logs.

☆U.S. GOVERNMENT PRINTING OFFICE: 1996 - 760-032/40008